United States
Environmental Protection
Agency

EPA-600/R-92-090

May 1992

EPA

Research and Development

SIMPLIFIED MODELING OF
AIR FLOW DYNAMICS IN
SSD RADON MITIGATION SYSTEMS
FOR RESIDENCES WITH GRAVEL BEDS

Prepared for

Office of Radiation Programs

Prepared by

Air and Energy Engineering Research
Laboratory
Research Triangle Park NC 27711

TECHNICAL REPORT DATA
(Please read Instructions on the reverse before complet

1. REPORT NO.	2.	3. PB92-195635
EPA-600/R-92-090		

4. TITLE AND SUBTITLE	5. REPORT DATE
Simplified Modeling of Air Flow Dynamics in SSD Radon Mitigation Systems for Residences with Gravel Beds	May 1992
	6. PERFORMING ORGANIZATION CODE: EPA/ORD
7. AUTHOR(S): T. A. Reddy, K. J. Gadsby, H. E. Black, III, D. T. Harrje, and R. G. Sextro	8. PERFORMING ORGANIZATION REPORT NO.: PU/CEES Report No. 246
9. PERFORMING ORGANIZATION NAME AND ADDRESS: Princeton University, Center for Energy and Environmental Studies, Princeton, New Jersey 08544	10. PROGRAM ELEMENT NO.
	11. CONTRACT/GRANT NO.: CR814673
12. SPONSORING AGENCY NAME AND ADDRESS: EPA, Office of Research and Development, Air and Energy Engineering Research Laboratory, Research Triangle Park, North Carolina 27711	13. TYPE OF REPORT AND PERIOD COVERED: Final; 8/89 - 2/91
	14. SPONSORING AGENCY CODE: EPA/600/13

15. SUPPLEMENTARY NOTES: AEERL project officer is Ronald B. Mosley, Mail Drop 54, 919/541-7865.

16. ABSTRACT: In an attempt to better understand the dynamics of subslab air flow, the report suggests that subslab air flow induced by a central suction point be treated as radial air flow through a porous bed contained between two impermeable disks. (NOTE: Many subslab depressurization systems, those now considered most effective for mitigating residences for radon, do not perform entirely satisfactorily, even when designed and installed by professionals.) The report shows that subslab air flow is most likely to be turbulent under actual field situations in houses with subslab gravel beds, but remains laminar when soil is present under the slab. The physical significance of a model is discussed, and simplified closed-form equations are derived to predict pressure and flows at various distances from a single central depressurization point. A laboratory apparatus was built to verify the model and experimentally determine the model coefficients of the pressure drop vs. flow for commonly encountered subslab gravel materials. These pressure drop coefficients can be used in connection with the simplified model as a rational way to assess subslab communication in houses. Preliminary field verification results in a house with gravel under the basement slab are presented and discussed.

17. KEY WORDS AND DOCUMENT ANALYSIS

a. DESCRIPTORS	b. IDENTIFIERS/OPEN ENDED TERMS	c. COSATI Field/Group
Pollution Radon Slabs Pressurizing Residential Buildings Gravel Mathematical Models Air Flow Dynamics	Pollution Control Stationary Sources Subslab Depressurization	13B 12A 07B 20D 13M, 13C 20K 14G 08G

18. DISTRIBUTION STATEMENT	19. SECURITY CLASS *(This Report)*	21. NO. OF PAGES
Release to Public	Unclassified	80
	20. SECURITY CLASS *(This page)*	22. PRICE
	Unclassified	

EPA Form 2220-1 (9-73)

EPA-600/R-92-090
May 1992

SIMPLIFIED MODELING OF AIR FLOW DYNAMICS IN SSD RADON MITIGATION SYSTEMS FOR RESIDENCES WITH GRAVEL BEDS

by

T.A. Reddy, K.J. Gadsby, H.E. Black, III,
D.T. Harrje, and R.G. Sextro

Center for Energy and Environmental Studies
Princeton University
Princeton, NJ 08544

EPA Cooperative Agreement CR-814673

EPA Project Officer
Ronald B. Mosley
Radon Mitigation Branch
Air and Energy Engineering Research Laboratory
Research Triangle Park, NC 27711

Prepared for
U. S. ENVIRONMENTAL PROTECTION AGENCY
OFFICE OF RESEARCH AND DEVELOPMENT
WASHINGTON, DC 20460

EPA REVIEW NOTICE

This report has been reviewed by the U.S. Environmental Protection Agency, and approved for publication. Approval does not signify that the contents necessarily reflect the views and policy of the Agency, nor does mention of trade names or commercial products constitute endorsement or recommendation for use.

This document is available to the public through the National Technical Information Service, Springfield, Virginia 22161.

ABSTRACT

The technique presently considered most effective for mitigating residences for radon is the subslab depressurization technique. Given that a large number of such mitigation systems designed and installed by the professional community do not perform entirely to satisfaction, there is a need to better understand dynamics of subslab air flow. In this report, it is suggested that subslab air flow induced by a central suction point be treated as radial air flow through a porous bed contained between two impermeable disks. Next, we show that subslab air flow is most likely to be turbulent under actual field situations in houses with subslab gravel beds, while remaining laminar when soil is present under the slab. The physical significance of this model is discussed and simplified closed-form equations are derived to predict pressure and flows at various distances from a single central depressurization point. A laboratory apparatus was built in order to verify our model and experimentally determine the model coefficients of the pressure drop versus flow for commonly encountered subslab gravel materials. These pressure drop coefficients can be used in conjunction with our simplified model as a rational means of assessing subslab communication in actual houses. Preliminary field verification results in a house with gravel under the basement slab are presented and discussed.

TABLE OF CONTENTS

Figures

Figures (continued)

Tables

GLOSSARY

Aggregate - crushed stone, stone, or other inert material or combinations thereof having hard, strong, durable pieces.

Air permeability (sub-slab) - a measure of the ease with which air can flow through a porous medium. High permeability facilitates air movement, and hence generally facilitates the implementation of soil-depressurization.

Basement - A Type of house construction where the bottom livable level has a slab (or earthen floor) which averages 3 ft or more below grade level on one or more sides of the house and is sufficiently high to stand in.

Coefficient of Determination (R^2) - This fractional measure represents the proportion of the total variability of the response variable that is explained by the relationship between the response variable and the exogenous variables.

Contractor - a building trades professional licensed by the state.

Crawlspace - an area beneath the living space in some houses, where the floor of the lowest living area is elevated above grade level. This space (which generally provides only enough head room for a person to crawl in), is not living space, but often contains utilities.

Depressurization - In houses, a condition that exists when the air pressure inside the house or in the soil is slightly lower than the air pressure outside. The lower levels of houses are almost always depressurized during cold weather, due to the buoyant force on the warm indoor air (creating the natural thermal stack effect). Houses can also be depressurized by winds and by appliances which exhaust indoor air.

Detached houses - Single family dwellings as opposed to apartments, duplexes, townhouses, or condominiums. Those dwellings which are typically occupied by one family unit and which do not share foundations and/or walls with other family dwellings.

Entry routes - Pathways by which soil gas can flow into a house. Openings through the flooring and walls where the house contacts the soil.

HAC system - A heating and air conditioning system. Typically residential because there is no intentional ventilation connected to the distribution system.

House air - Synonymous with indoor air. The air that occupies the space within the interior of a house.

Indoor air - That air that occupies the space within the interior of a house or other building.

Livable space - Any enclosed space that residents now use or could reasonably adapt for use as living space.

Mean (arithmetic) - The mean of a set of quantitative data is equal to the sum of the measurements divided by the number of measurements.

Mitigation - The act of making less severe, reducing or relieving. For the purposes of this standard, a building shall not be considered as *mitigated* until it has been demonstrated to comply with applicable limits of indoor radon concentration.

Outside air - air taken from the outdoors and, therefore, not previously circulated through the system.

Permeability - (see air permeability).

Picocurie (pCi) - A unit of measurement of radioactivity. A curie is the amount of any radionuclide that undergoes exactly 3.7×10^{10} radioactive disintegrations per second. A picocurie is one trillionth (10^{-12}) of a curie, or 0.037 disintegrations per second.

Picocurie per liter (pCi/L) - A common unit of measurement of the concentration of radioactivity in a fluid. A picocurie per liter corresponds to 0.037 radioactive disintegrations per second in every liter of air.

Radon - The only naturally occurring radioactive element which is a gas. Technically, the term "radon" can refer to any of a number of radioactive isotopes having atomic number 86. In this document, the term is used to refer specifically to the isotope radon-222, the primary isotope present inside houses. Radon-222 is directly created by the decay of radium-226, and has a half-life of 3.82 days. Chemical symbol Rn-222.

Soil depressurization system - a system designed to withdraw air below the slab through means of a vent pipe and fan arrangement (active) or a system designed to lower sub-slab air pressure by use of a vent pipe to the outside but relying solely on convective air flow of upward air in the vent (passive).

Soil gas - Gas which is always present underground, in the small spaces between particles of the soil or in crevices in rock. The major constituent of soil gas is air with some components from the soil (such as radon) added.

Stack effect - The upward movement of house air when the weather is cold, caused by the buoyant force on the warm house air. House air leaks out at the upper levels of the house, so that outdoor air (and soil gas) must leak in at the lower levels to compensate. The continuous exfiltration upstairs and infiltration downstairs maintain the stack effect air movement, so named because it is similar to hot combustion gases rising up a fireplace or furnace flue stack.

Standard deviation - This is statistical measure of dispersion, defined as the positive square root of the mean of squares of deviations from the mean.

Ventilation - the process of supplying or removing air, by natural or mechanical means, to or from any space. Such air may or may ot have been conditioned.

METRIC EQUIVALENTS

Metric	Multiply by	Yields nonmetric
centimeter (cm)	0.39	inch (in)
centimeter (cm)	0.033	foot (ft)
meter (m)	3.28	foot (ft)
square meter (m^2)	10.76	square foot (ft^2)
liter (L)	0.35	cubic ft (ft^3)
cubic meter (m^3)	35.31	cubic ft (ft^3)
liter per second (L/sec)	2.11	cubic foot per minute (cfm)
Pascal (Pa)	0.004	inch of water column (in WC)
Becquerel per cubic meter (Bq/m^3)	0.027	picocurie per liter (pCi/L)
degree Centigrade (°C)	(9/5°C)+32	degree Fahrenheit (°F)

Nomenclature

A	cross-sectional area of flow
a	parameter representive of the resistivity to flow of the porous bed
b	exponent appearing in eq.(3b)
c	dimensionless constant appearing in eq.(3a)
d	diameter
d_v	equivalent diameter of pebbles
F	correction factor given by equation (17b)
f	friction factor
g	acceleration due to gravity
h	thickness of the porous bed
K	parameter representative of the conductivity to flow of the porous bed
K_p	pressure loss coefficient at entry to suction pipe
k	permeability of porous bed
L	length of pipe
n	exponent appearing in eq.(3a)
Δp	pressure drop
p	pressure
p_a	atmospheric pressure
q	total volume flow rate
R^2	coefficient of determination of regression
Re	Reynolds number
r	radial distance from center of the suction hole
r_o	outer radius of the laboratory apparatus
SEM	standard error of the mean of the regression estimate
V	air velocity

x	distance along flow
α	opening angle of porous bed through which radial flow occurs
ρ	density
ν	kinematic viscosity
μ	dynamic viscisity
ϕ	porosity of porous bed

Suffix

a	air, ambient
b	porous bed
ent	entrance
f	fluid
p	pipe
w	water

ACKNOWLEDGMENTS

The assistance of R. Gafgen and R. de Silva during the experimental phase of this study is acknowledged as also is that of D. Hull for his insight into certain statistical aspects. Fruitful discussions and insights into fundamental hydrological concepts by Prof. G.F. Pinder and J. Guarnaccia were invaluable during the initial stages of this study. Critical comments, encouragement, and indepth reviews of the manuscript by R. Mosley, D. Sanchez, and L. Sparks of U.S. EPA, AEERL, are acknowledged.

1. Introduction

The presence of radon 222, a colorless, odorless gas naturally present in trace concentrations in soil gas and underground water has been found to be a serious health hazard in many American houses. Generally, radon-contaminated soil gas enters a home through cracks and openings in the slab being driven by pressure differences between the subsoil and the basement and walls, or between the subsoil and the living area in case of a slab-on-grade house construction. These pressure differences occur naturally, either because of stack (i.e. temperature difference) or wind effects, or due to zonal depressurization due to the effect of the heating and air-conditioning system (HAC). The Environmental Protection Agency (EPA) and other health organizations have recognized the health risk of elevated indoor radon concentrations and have set a guideline of 148 Bq/m^3 (4 pCi/L) as a radon level beyond which mitigation is recommended. It is estimated that up to 10 million US homes have elevated indoor radon concentrations. Thus there is a need to ensure the effectiveness and proper design of mitigation systems.

An EPA sponsored workshop was held at Princeton University in order to summarize available knowledge on various radon diagnostic techniques [1]. Four phases of radon diagnostics were defined:

(a) Radon problem assessment diagnostics involving radon source strength, location, house characteristics, and house occupancy characteristics.

(b) Pre-mitigation diagnostics entailing the selection of the best mitigation system for the particular building taking into account radon source strength and location, particularly at the substructure.

(c) Mitigation installation diagnostics used during installation of mitigation systems in order to assure proper operation.

(d) Post-mitigation diagnostics to assure that the radon guidelines have been met and

that the mitigation system is adjusted properly.

The emphasis of the workshop was on diagnostics since each home, housing division, and region has different radon characteristics which require that special attention be paid to system design in order to maximize mitigation performance and minimize cost. This issue was of particular importance since it was found that a large number of houses which had been mitigated still had elevated radon levels. In fact, a recent study [2] found that 64% of the homes in New Jersey where post-mitigation radon measurements have been made, remained above 148 Bq/m^3 (4 pCi/L). Diagnostics are therefore crucial for providing information relevant and necessary to the successful design and implementation of a radon mitigation system.

Many participants of the workshop felt that radon mitigation via subslab depressurization (SSD) was the best approach for houses with a gravel bed. Surveys indicate that systems based on this technique account for more than 50% of all installed systems [3]. (Another promising technique involves subslab pressurization. Since the two techniques are similar in terms of subslab dynamics of induced air flow, they can both be treated in the same scientific framework.) In the pre-mitigation diagnostic phase, the degree of communication under the slab as well as the permeability characteristics of the subslab medium must be determined before appropriate depressurization conditions can be determined. Proper attention to these aspects will ensure that reasonable flows, and hence the desired degree of depressurization, will prevail at all points under the slab. Lowering the pressures at all points of the subslab to values below those of the basement/crawl-space/living area will subsequently reduce radon-rich soil-gas from moving or seeping into the building by convection.

Parallel with the above aspect is the concern that presently mitigators tend to over-design SSD systems in order to err on the safe side. In so doing, more radon from the

soil is removed and vented to the ambient air than would have occured naturally. There is thus a prudent need to downsize current overly robust SSD mitigation systems and decrease emission exhaust quantities of radon while simultaneously ensuring that indoor radon levels do not exceed the desired concentrations.

The Center for Energy and Environmental Studies of Princeton University is currently involved in the formulation and verification of a rapid diagnostic protocol for subslab and wall depressurization systems designed to control indoor radon levels [4]. It is hoped that the protocol would lead not only to the ability to distinguish between homes that are hard or easy to mitigate, but also to the articulation of a more rational and scientific approach which would be especially useful to the ever-increasing body of professional radon mitigators. Other researchers have or are also addressing this issue of optimal SSD design [5 - 7].

Our approach to the formulation of the diagnostics protocol consists of:

(1) a practical component, in that specific guidelines would be provided so that the effectiveness of the engineering design of the radon mitigation system would be enhanced, and

(2) scientific studies at a more fundamental level which would validate and provide quantitative guidelines more rationally.

The scientific component would involve improved understanding of those factors governing the pressure-induced air flow beneath the concrete slab in order to predict and then optimize the pressure field extension patterns induced by single and multiple suction points. The present study specifically addresses the former aspect, while the latter would be dealt with in a subsequent study.

2. Conclusions

The important features of this study are as follows:

(a) We have outlined the general problem of radon mitigation system design and discussed the scope and limitations of prior studies in both this aspect and also at a more fundamental aerodynamical level. The first problem should be to determine the nature of air flow below the concrete slab and how this is likely to affect the pressure drop versus flow correlation for given subslab conditions.

(b) Next we give arguments to support the suggestion of a prior study (Ref. [8]) that flow under the slab of a house during mitigation using the subslab depressurization (and the pressurization) technique be likened to radial flow between two impermeable disks.

(c) We point out that subslab air flow under actual operation of mitigation systems is likely to be turbulent if a gravel bed is present and laminar in the presence of soil.

(d) We then present a mathematical treatment to analytically predict the pressure field in homogeneous circular porous beds when subjected to a single central suction hole.

(e) A laboratory apparatus constructed so that it can specifically duplicate conditions which occur in practice under slabs of real houses being mitigated for radon using the depressurization (or the pressurization) technique) is then described. The experimental procedure followed in order to measure the pressure field of turbulent air flow is outlined from which the regression coefficients of the pressure drop versus flow correlation can be determined.

(f) Preliminary field verification results of our modeling approach in a house with gravel under the basement slab are presented and discussed. A striking conclusion of our study is that even a visual inspection of the porous material under the slab may be an indicator good enough for a sound engineering design, if used in parallel with our

modeling approach and given a table containing the aerodynamic pressure drop coefficients of commonly found subslab material.

(g) How closed form equations can be used to generate design figures useful to the practical mitigator has also been illustrated.

(h) Practical notions regarding proper piping design of the mitigation system in view of pressure drop considerations have finally been addressed.

3. Specification of the Problem

In terms of modeling the induced subslab pressure fields, one could conceptually divide the present housing stock construction into broadly three groups: (i) those with a gravel bed under the concrete slab, (ii) those without, in which case soil is the medium under the slab, and (iii) those houses which have both. In the case of (ii), the subslab permeabilities are much lower than for case (i) requiring more careful design of the mitigation system. In New Jersey, houses less than about 30 years old typically have gravel beds of about 0.05-0.1 m (2 in.-4 in.) under the slab. However other states seem to have very different construction practices: for example, houses in Florida and New Mexico are built directly on compacted fine-grained soil which offers high resistance to air flow [5-7].

Fig. 1 schematically depicts the type of construction and the expected air flow paths one would typically expect in a house with a gravel bed when a single suction point through the slab is used to induce a pressure field. In case of a radon mitigation system using subslab pressurization, one could, to a good approximation, simply assume similar aerodynamic effects with the direction of air flows reversed. Since the permeability of the gravel bed is usually very much higher than that of the soil below, one could assume, except for the irregular pattern around the footing which would occur over a relatively small length, that the subslab air flow is akin to radial flow between two impermeable

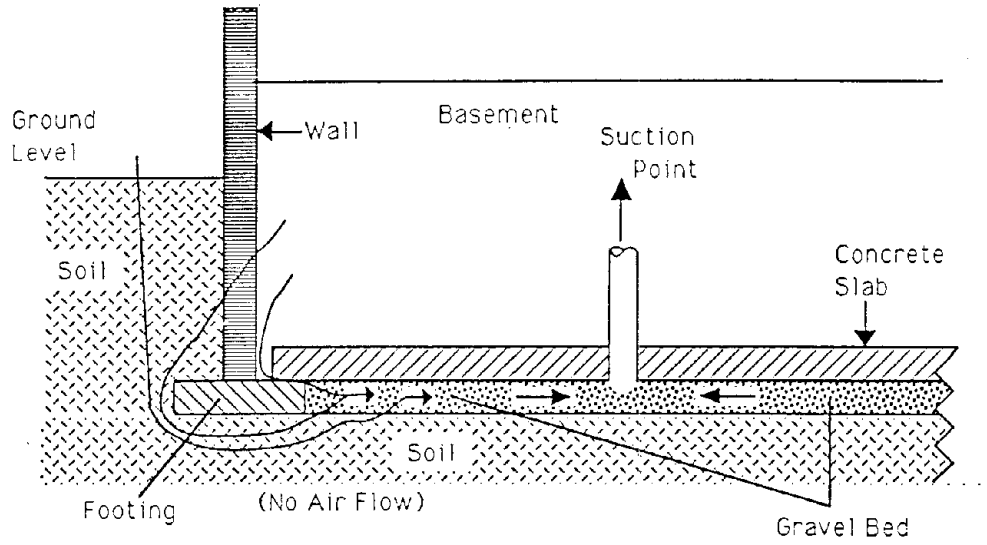

Fig. 1 Schematic of subslab air flows in a house with a gravel bed when the house is being mitigated following the subslab depressurization technique. Note that part of the air flowing through the gravel bed originates from the basement and the rest from the ambient air.

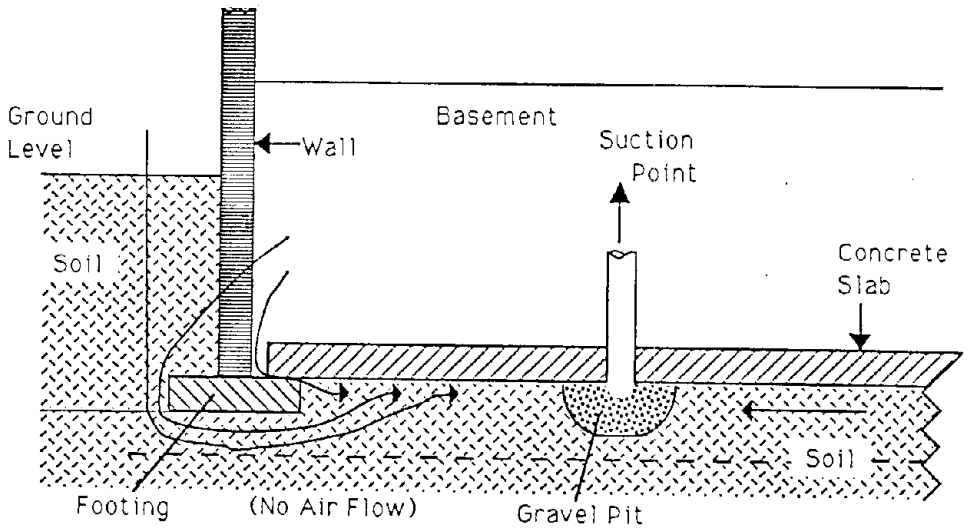

Fig. 2 Schematic of subslab air flow in a house without a gravel bed when the house is being mitigated following the subslab depressurization technique.

circular disks with a spacing equal to the thickness of the gravel bed. Note that this model equally accounts for the leakage of air from the basement which essentially occurs from the perimeter cracks.

In case of a house without a gravel bed, suction applied at a simple penetration through the slab (as in Fig. 1) is no longer practical in low permeability soils since the area of depressurization is small. In order to enhance mitigation effectiveness, the contemporary thinking is to increase this area of depressurization by either digging a gravel pit below the concrete slab as shown in Fig. 2, or more simply, by hollowing out a hemisphere of about 0.3-0.45 m (12 in.-18 in.) radius underneath the suction hole. Even under such conditions, and provided the soil underneath is free of major obstructions like concrete footings, duct work, piping, and large rocks, one could view air flow as occurring between two impermeable circular disks with a spacing equal to either the depth of the gravel pit or the radius of the hollow hemisphere.

The above discussion was intended primarily to suggest that flow underneath the slab be visualized as occurring in radial streamlines terminating at the central suction point. Note that such a representation would perhaps be too simplistic or even incorrect for a house with a partial-basement (case (iii) above). In the present study, we shall limit ourselves to understanding the flow and pressure drop characteristics through a homogeneous bed (of either gravel or sand) with uniform boundary conditions, the obvious case to start with being a circular configuration.

The first question to be addressed relates to the nature of the flow, i.e., whether the flow is laminar or turbulent, and whether there is a transition from one regime to another.

As outlined in Appendix A, where a brief overview of the basic scientific theory of flow through porous beds is given, the Reynolds number gives an indication of the flow

regime. Though there is an inherent ambiguity in the definition of the quantity characterizing the length dimension, we shall adhere to the following definition:

$$Re = \frac{q}{A} \cdot \frac{1}{\nu_a} \cdot \frac{d_v}{\phi} \qquad (1)$$

where q - total volume flow rate,

A - cross-sectional area of flow (in the case of radial flow through a circular bed of radius r and thickness h, the area = $2\pi rh$),

ν_a - kinematic viscosity of air,

d_v - equivalent diameter of pebbles, and

ϕ - void fraction or porosity of the gravel bed.

Let us first look at flow through a gravel bed. Some typical values of the above parameters could be assumed:

h = 0.1 m (4 in.), d_v = 0.0125 m (1/2 in.), ν_a (at 15°C) = 14.6×10^{-6} m/s, and ϕ = 0.4.

The values of q encountered in practice range from 9.4×10^{-3} to 47.2×10^{-3} m^3/s (20-100 cfm). Under these conditions, the resulting Reynolds number for radial flow at different radii can be determined from eq. (1) or Fig.3. From Appendix A, we note that a safe lower limit for turbulent flow is when Re >10, and a safe upper limit for laminar flow is when Re < 1.[1] Since basements do not generally exceed 6 m (20 feet) in radius, we note from Fig.3 that subslab flow would tend to be largely turbulent when a gravel bed is present. This by itself is an important finding since explicit recognition does not seem

[1]The common held conception that turbulent flow occurs at Reynolds numbers of several thousands is valid only for flow inside tubes and ducts and not for flow in packed beds.

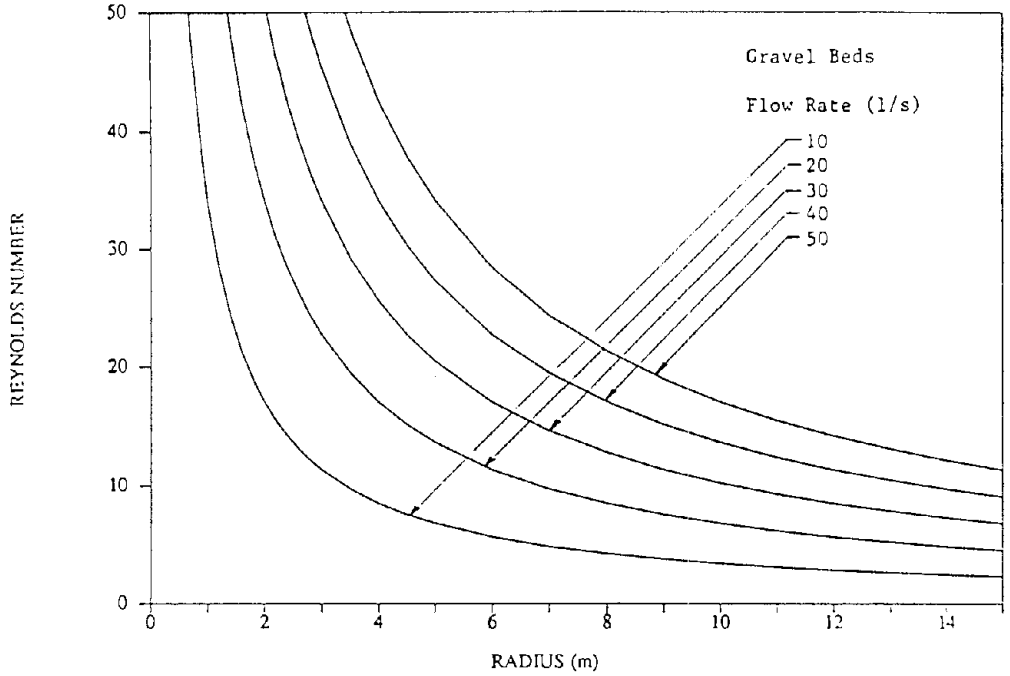

Fig. 3 Expected Reynolds number for air flows through subslab gravel beds of houses being mitigated for radon. A radial cylindrical disk flow with impermeable boundaries is assumed with disk spacing = 0.1 m (4 in.), diameter of gravel = 0.012 m (1/2 in.) and porosity of bed = 0.4. (Reynolds numbers above 10 indicate turbulent flow while those below 1 correspond to laminar flow.)

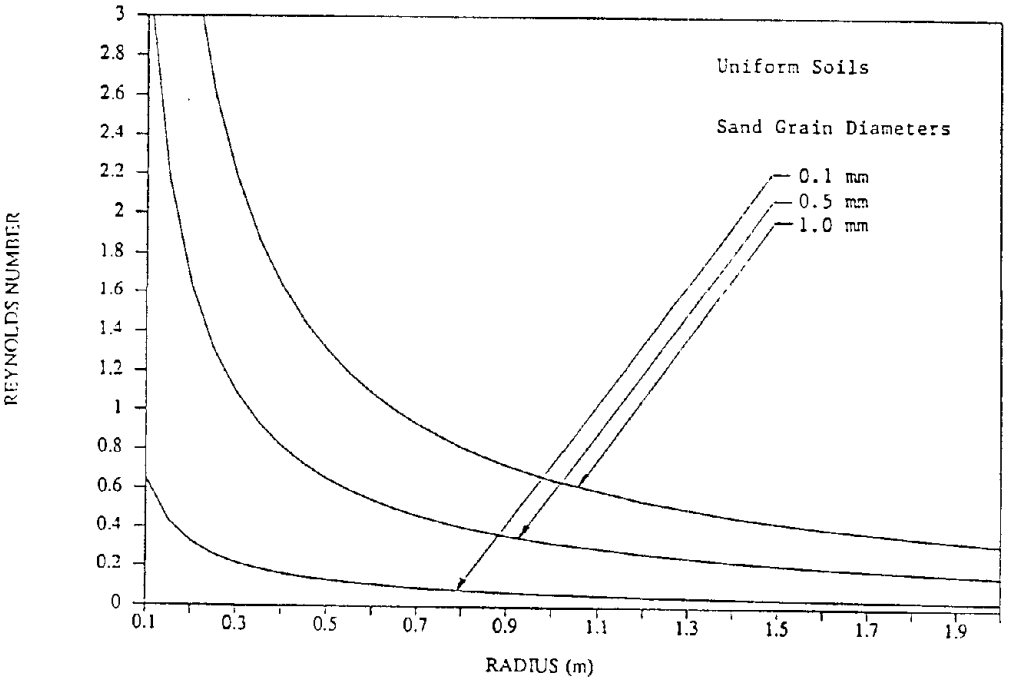

Fig. 4 Expected Reynolds number for air flows through subslab soil beds of houses being mitigated for radon. A radial cylindrical disk flow with impermeable boundaries is assumed with disk spacing = 0.1 m (4 in.), flow rate = 2.36 l/s (5 cfm) and porosity of bed = 0.4. (Reynolds numbers below 1 indicate laminar flow while those between 1 and 10 correspond to transition range.)

to have been made of this aspect in earlier studies.

The usefulness of Fig.3 can be extended to cover other types of circular configurations. Thus if one would like to estimate Re numbers for radial flow through a slice with impermeable sides and with an opening angle α instead of an entire pie-configuration, one needs simply to use the following correction:

$$Re\alpha = Re_{360} \cdot (360/\alpha) \qquad (2a)$$

where Re_{360} is read from Fig.3.

Also if the disk spacing is not 0.1 m (4 in.) but say h', the Reynolds number can be obtained from Fig.3 corresponding to an effective radius r' in meters given by:

$$r' = r \cdot (0.1 / h') \qquad (2b)$$

Similar corrections can be made to other parameters as well. Thus, in conclusion, we should expect turbulent flow conditions to prevail through subslab gravel beds during normal operation of mitigation systems using the subslab depressurization (or pressurization) technique. On the other hand, in a house with soil as the subslab medium, this observation is no longer valid. Grain diameters of sand range from 0.06 to 2 mm (0.0024-0.08 in.) [9] while volume flow rates in corresponding mitigation systems are typically lower, about 0.83×10^{-3}-6.2×10^{-3} m^3/s (2-15 cfm). Assuming some typical values of h = 0.1 m (4 in.), ϕ = 0.4 and q = 2.4×10^{-3} m^3/s (5 cfm), the corresponding Reynolds numbers for air flow through sands of different grain diameters have been calculated from eq.(1) and are shown in Fig. 4. We note that the flow is likely to be laminar in most cases.

Finally, we present Figs. 5 and 6 in order that the reader acquire a feel for the range of air flow velocities which would induce the values of Reynolds numbers seen in Figs. 3

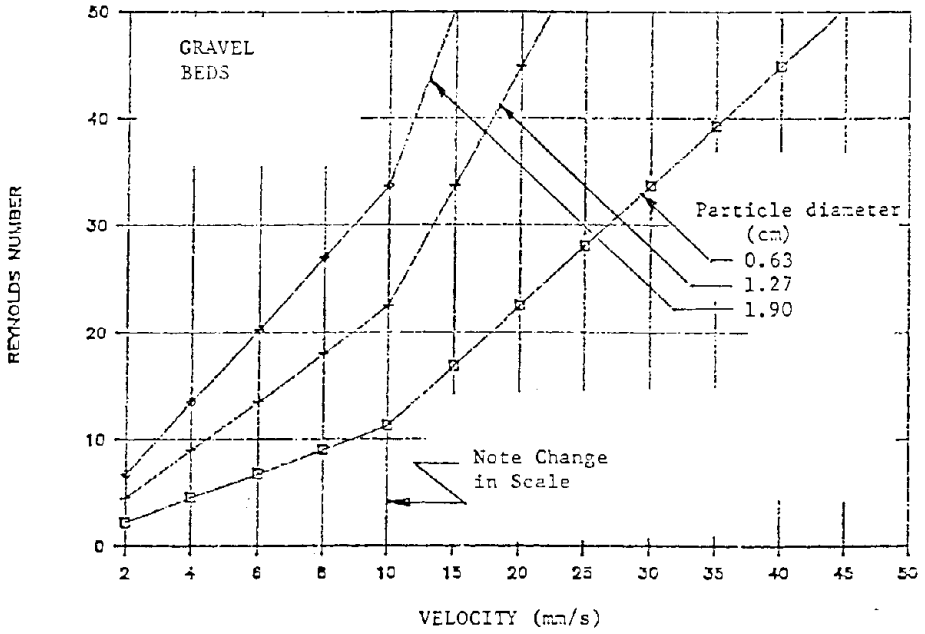

Fig. 5 Variation in Reynolds number of air flow through a porous media for different superficial air velocities. The porous media is assumed to have a porosity of 0.4, and the three different values of particle diameter relate to gravel beds.

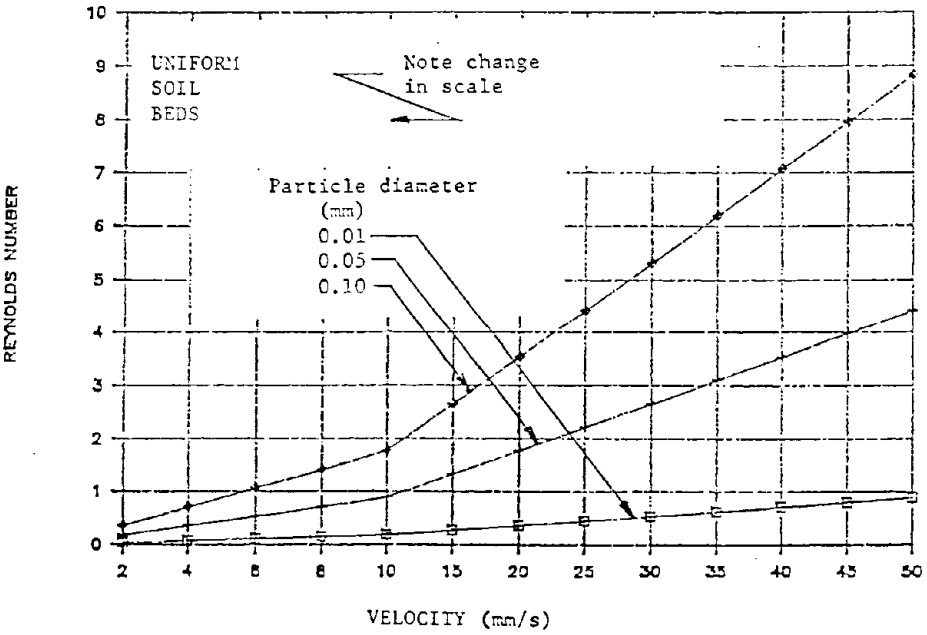

Fig. 6 Variation in Reynolds number of air flow through a porous media for different superficial air velocities. The porous media is assumed to have porosity of 0.4, and the three different values of particle diameter relate to sand beds.

and 4. These have been computed from eq.(1) for different values of particle diameters corresponding to both gravel and sand beds. We note that even with very small velocities of the order of a few millimeters per second, flow is likely to be turbulent.

4. Mathematical Model for Radial Flow

At the onset, let us mention that there are essentially two different problems involved with modeling the inflow of radon-enriched air into a residence. One problem is associated with flow through openings in the slab resulting from small pressure differences impressed across the concrete slab due to environmental driving forces (stack effect, wind and HAC operation). The other problem involves modeling the air flow under the concrete slab when relatively large pressure differentials are applied at one, or several, perforations through the slab (conditions that arise when houses are being mitigated). Though both these problems essentially involve modeling the air flow through the ground under the slab, the difference is that the dynamics and entry paths are entirely different: flow paths and flow regimes (both in soil and into the basement) and external factors causing flow will be widely different in both. The pressure differences in the former (i.e., flow occurring naturally in the absence of a suction pressure) are so small that the assumption of a laminar flow is usually valid, and effects like diffusion through soil and via small capillary cracks into the basement have to be considered [15]. In the case of the latter, the flow regime in gravel beds will most probably be turbulent and the flow paths of radon enriched air will be predominantly towards the suction hole.

As a result of these differences, studies or models pertaining to one problem cannot be applied as such to the other. There are a number of studies which have addressed the first problem (e.g., Refs. [10-14]) while studies relating to the latter are very few. We could only find two relevant studies; one numerical study using a finite difference computer model [7], and the other an empirically based study [8]. The principal

drawbacks of Refs. [7,14] are that laminar flow is assumed and the computer code may be difficult to use and to transfer to other research groups. Moreover, a certain amount of effort is required in order that the results of such codes be useful to practitioners.

The core of any model is the formulation of the structure of a correlation between pressure drop and Reynolds number. There is an abundance of literature relating to flow through porous media as evidenced by the large number of books and monographs on this topic (e.g., [16-21]). A major portion of this literature relates to laminar flow where Darcy's Law holds (see Appendix A for explanation). This fact is not too surprising since flow characteristics in petroleum and gas fields, or water flow in subsoils, or decontamination of subsoil acquifers, were some of the problems which historically led to the scientific treatment of flow through porous media. Subsequently, this was extended to various other problems such as flow through fluidized and packed beds, both in chemical kinetics and in areas involving drying of cereal grains and sensible heat storage. We have made a preliminary search through such literature and find that one cannot directly adopt a particular correlation as such to the present problem though insight into the type of needed model structure can be gained.

Consequently, (this is further discussed in Appendix A), we have adopted in the present study the following simple model structure for the onset of turbulent flow.

$$Re \cdot f^n = c \tag{3a}$$

where f is the friction factor of the porous bed and c and n are empirical dimensionless coefficients.

In Appendix A (see eqs.(A16 and A17)), we show that this model structure is identical to the following model:

$$\frac{1}{\rho_f g} \cdot \frac{dp}{dx} = a \cdot \left(\frac{q}{A}\right)^b \tag{3b}$$

where the left-hand side is the pressure drop in head of the flowing fluid per unit bed length. The parameter a can be loosely interpreted as the resistivity of the porous bed to the flow of the particular fluid.

Theory predicts a value of unity for the exponent b when the flow is laminar (we then have the Darcy Law), and a value nearer to 2 when the flow is turbulent. Given the irregularities both in shape and size prevalent in gravel beds below the concrete slab, the coefficients should be determined from regression to actual data obtained by experiments on the specific bed material. The real objective of this study is thus to gauge the accuracy of such a model structure when applied to house-like conditions. Note also that the effective permeability[2] k of a porous bed [see eqs.(A9-A12) of Appendix A] can be easily deduced from the coefficient a of eq.(3b), since

$$k = \frac{\nu_a}{g} \cdot \frac{1}{a} \tag{4}$$

where ν_a is the kinematic viscosity of air.

Ref. [8] also uses a model like that of eq.(3) with, however, the parameters transposed, i.e. (q/A) expressed as a function of the pressure drop gradient. It is trivial to go from one form to another but we find it more convenient to work with an equation like eq.(3b).

---

[2]We use the term 'effective permeability' instead of permeability, only because of the uncertainty involved in the extrapolation from the present experimental data (done under turbulent flow) to Darcy flow (i.e., laminar flow conditions) under which permeability is conventionally defined. This aspect is further discussed in Section 6.

We shall now seek to derive a mathematical expression for the pressure field when air flows radially through a circular homogeneous gravel bed when suction is applied at the center of the circle. The laws of conservation of matter and of energy must be satisfied in any hydrodynamic system. By setting viscosity terms to zero in the Navier-Stokes equations we get the Euler equation of motion. For the suction pressures encountered in this particular problem, air can be assumed to be an incompressible fluid and we have Bernouilli's equation, which in differential form is:

$$\frac{d}{dr}\left(\frac{1}{2g}V^2(r) + \frac{p(r)}{g.\rho_a}\right) = 0 \qquad (5)$$

where ρ_a is the density of air, V the superficial velocity and p(r) the pressure of air at a radial distance r from the center. Strictly, the distance should be taken from the outer edge of the suction pipe (r' in Fig. 7). The diameter of the suction pipe is typically so small that one could neglect this difference without any error in the subsequent analysis.

Assuming that energy or pressure drop (in units of head of air) lost as a result of viscous drag by the gravel bed can be simply treated as an additive term, we have

Total pressure drop = Pressure drop due to changing cross-section + Pressure drop due to viscous drag

Assuming a simple model such as eq.(3b) yields

$$\frac{d}{dr}\left(\frac{p(r)}{\rho_a.g}\right) = -\frac{d}{dr}\left[\frac{1}{2g}\cdot\left(\frac{q}{2\pi h}\right)^2\cdot\frac{1}{r^2}\right] + a\cdot\left(\frac{q}{2\pi h}\right)^b\cdot\frac{1}{r^b} \qquad (6)$$

Integrating eq.(6), we have

$$\frac{p(r)}{\rho_a.g} = a\cdot\left(\frac{q}{2\pi h}\right)^b\cdot\frac{r^{1-b}}{(1-b)} - \frac{1}{2g}\cdot\left(\frac{q}{2\pi h}\right)^2\cdot\frac{1}{r^2} + \text{constant} \qquad (7)$$

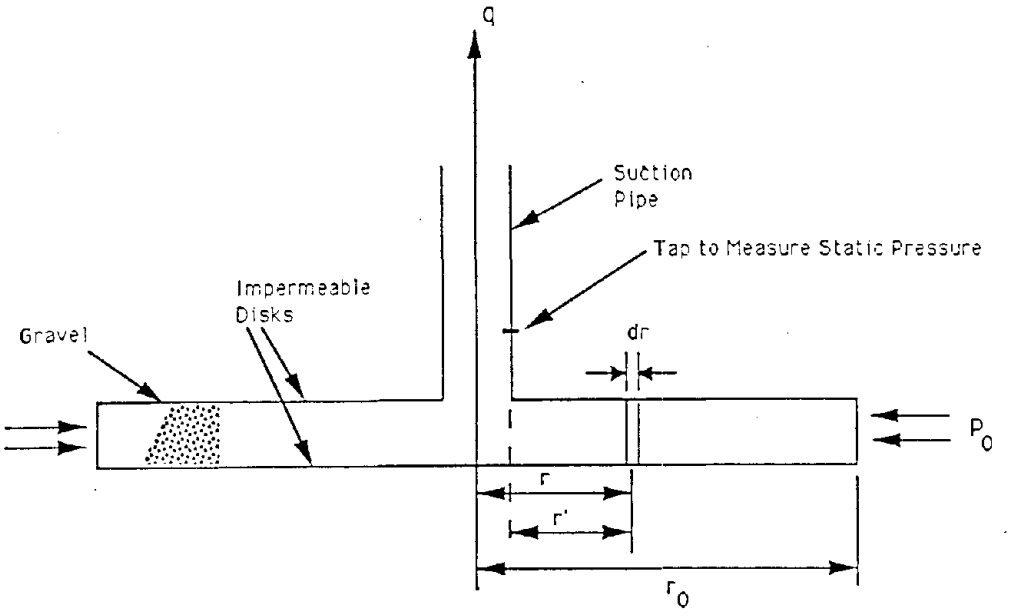

Fig. 7 Schematic of a model to duplicate flow conditions occurring beneath the concrete slab of a residence when induced by a single suction point. The air flow is assumed to be radial flow through a homogenous porous bed of circular boundary.

The constant of integration can be found from the boundary conditions.

At the outer fringe of the cylindrical disk:

$r = r_o$, $p = p_a$ (the atmospheric pressure).

Introducing this into eq.(7), the following expression for the pressure drop is obtained

$$\frac{p(r)-p_a}{\rho_a.g} = a \cdot \left(\frac{q}{2\pi h}\right)^b \cdot \frac{1}{(1-b)} \cdot (r^{1-b}-r_o^{1-b}) - \frac{1}{2g} \cdot \left(\frac{q}{2\pi h}\right)^2 \cdot \left(\frac{1}{r^2} - \frac{1}{r_o^2}\right) \qquad (8)$$

Note that the expression [p(r) - p_a] is a negative quantity which represents the suction pressure, i.e., the pressure below the ambient pressure.

Since the pressure drop is often measured in units of head of water, it is more convenient to modify the above equations into:

$$\frac{p(r)-p_a}{\rho_w.g} = a \cdot \frac{\rho_a}{\rho_w} \cdot \left(\frac{q}{2\pi h}\right)^b \cdot \frac{1}{(1-b)} \cdot (r^{1-b}-r_o^{1-b}) - \frac{1}{2g} \cdot \frac{\rho_a}{\rho_w} \left(\frac{q}{2\pi h}\right)^2 \cdot \left(\frac{1}{r^2} - \frac{1}{r_o^2}\right) \qquad (9)$$

We note that the second term on the R.H.S. of eq.(9) relates to the pressure drop arising simply as a result of decreasing cross-sectional area in the direction of flow (which is radially inward) while the first term accounts for the viscous drag due to the gravel bed. In case (and this will normally be so, as we shall see in the next section) the viscous drag term is very much larger than the former effect, the above equation simplifies into:

$$\frac{p(r)-p_a}{\rho_w.g} = \frac{1}{k} \cdot \frac{\nu_a}{g} \cdot \frac{\rho_a}{\rho_w} \cdot \left(\frac{q}{2\pi h}\right)^b \cdot \frac{1}{(1-b)} \cdot (r^{1-b}-r_o^{1-b}) \qquad (10)$$

Note that k is an effective permeability defined in eq.(4).

The above equation predicts the pressure field for a pre-specified total air flow rate q. In case one wishes to predict the resulting flow rate for an imposed suction pressure, the above equation can still be used by simply rearranging the appropriate terms.

It is clear that the derivation is easily modified in case one wishes to either assume another model structure for the pressure drop correlation [i.e., eq.(3)], or even when the flow is through a homogeneous circular bed with impermeable sides and segmented into an angle α as against 360°. The expression $(q/2\pi h)$ simply needs to be modified appropriately.

For the special case of b=2, eq.(9) transforms into:

$$\frac{p(r)-p_a}{\rho_w.g} = -\left[a \cdot \left(\frac{1}{r} - \frac{1}{r_o} \right) + \frac{1}{2g} \cdot \left(\frac{1}{r^2} - \frac{1}{r_o^2} \right) \right] \cdot \frac{\rho_a}{\rho_w} \cdot \left(\frac{q}{2\pi h} \right)^2 \qquad (11)$$

On the other hand, during <u>laminar flow</u>, Darcy's Law holds and the exponent b=1. Moreover during such cases, the pressure drop due to changing cross-section is essentially negligible as compared to the pressure drop due to viscous drag offered by the particles of the porous bed (see for example, [16]). Under these circumstances, the expression for the radial pressure drop in a circular porous bed is given by

$$\frac{p(r)}{\rho_a.g} = a \cdot \frac{q}{2\pi h} \int \frac{1}{r} \, dr \qquad (12)$$

which, on integration and on introducing the boundary conditions yields

$$\frac{p(r)-p_a}{\rho_w.g} = a \cdot \frac{\rho_a}{\rho_w} \cdot \frac{q}{2\pi h} \cdot \ln \left(\frac{r}{r_o} \right) \qquad (13a)$$

$$= \frac{\nu_a}{g} \cdot \frac{1}{k} \cdot \frac{\rho_a}{\rho_w} \cdot \frac{q}{2\pi h} \cdot \ln\left(\frac{r}{r_o}\right) \qquad (13b)$$

It is easy to modify these equations to apply to outward radial flow as one would encounter in houses where the subslab pressurization technique is used. The boundary conditions are still the same but now the pressure at the throat of the suction pipe is higher than ambient pressure and the quantity $[p(r) - p_a]$ is positive and represents the pressure above the ambient pressure. The final expression analogous to eq.(9) is:

$$\frac{p(r)-p_a}{\rho_w \cdot g} = -a \cdot \frac{\rho_a}{\rho_w} \cdot \left(\frac{q}{2\pi h}\right)^b \cdot \frac{1}{(1-b)} \cdot (r^{1-b} - r_o^{1-b}) - \frac{1}{2g} \cdot \frac{\rho_a}{\rho_w} \cdot \left(\frac{q}{2\pi h}\right)^2 \cdot \left(\frac{1}{r^2} - \frac{1}{r_o^2}\right) \qquad (14)$$

Another instance where our approach is directly applicable is when the porous bed consists of two or more types of porous material. For example, one could come across a house construction where the subslab gravel bed consists of two horizontally distinct layers of gravel of different sizes. The above equations can be easily modified to apply to such cases as well.

The practical implications of the parameters k and b are that if they are really constant for a given bed material and can be determined by actual experiments in the field, they will serve as indices by which a mitigator will be able to assess how much of the area from the suction hole he can hope to access for a given suction pressure.

The irregular boundary conditions that arise in practice are however not easily tractable with a simple expression such as eq.(9), and resorting to a numerical computer code may be the only proper way of proceeding in order to predict resulting pressure fields. Another problem in applying an approach such as the above to practical situations may be the drastic departure from homogeneity in certain subslab gravel beds (as also in the

case of subslab soil beds). How influential these problems are in real situations is addressed to some extent in section 7.

5. Laboratory Apparatus

One needs to evaluate the soundness of the mathematical derivation presented above and also to determine the numerical values of the empirical coefficients of eq.(3b). To this end, a laboratory model consisting of a 2.4 m (8 ft) diameter circular section that is 0.15 m (6 in.) deep was constructed as is schematically shown in Fig. 7. The top and bottom impermeable disks were made from 0.02 m (3/4 in.) thick plywood, and a wire mesh at the outer periphery of the disks was used to contain the gravel between the two disks (Fig. 8). The apparatus allowed experiments to be conducted with a maximum disk spacing (or depth of gravel bed) of 0.095 m (3.75 in.). An open-cell foam sheet 0.025 m (1 in.) thick was glued to the underside of the top plywood disk. It was hoped that during experiments heavy weights placed on top of the plywood disk would effectively eliminate gaps that may exist between the disk and the gravel top that could cause short-circuiting of the air flow. In so doing, we hoped to guarantee that air flow occurs through the bed and not over it.

A 0.038 m (1.5 in.) diameter hole was drilled at the center of the top disk to serve as the suction hole. Nine holes, whose layout is shown in Fig. 9, were drilled on three separate rays of the top disk and a PVC pipe of 0.012 m (1/2 in.) inner diameter with chamfered ends was tightly squeezed into these holes. Pressure measurements at these nine holes would then yield an accurate picture of the pressure field over the entire bed.

The total volume of the packed bed is approximately 0.43 m^3 (16 ft^3) which, for river-run gravel, translates into a net weight of about 700 kg (1530 lb).

Equipment needed for the experiments included:

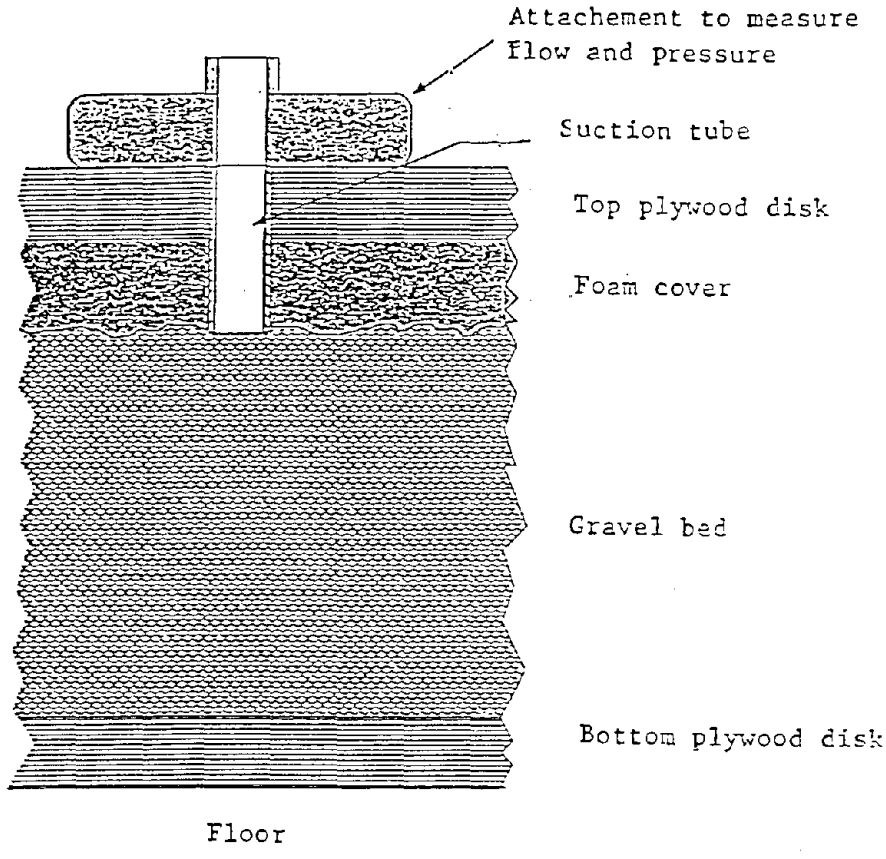

Fig. 8 Cross-section of the experimental laboratory apparatus.

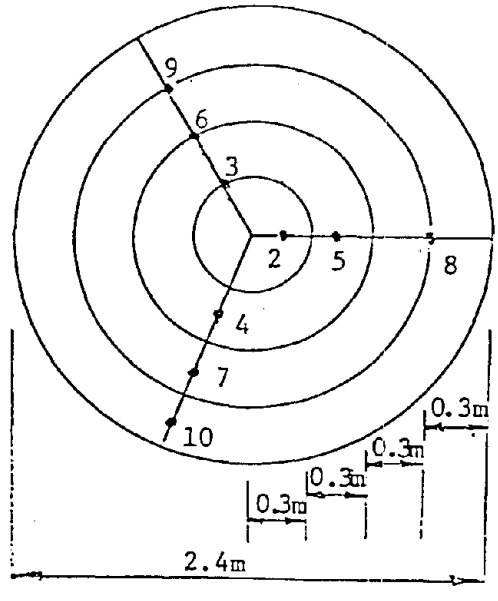

Fig. 9 Layout of the test holes to measure static pressures in the porous bed.

(i) an industrial vacuum cleaner capable of sucking 45 x 10^{-3} m^3/s (95 cfm) of air through a 0.05 m (2 in.) diameter orifice under 1.9 m (75 in.) of water static vacuum pressure;

(ii) a speed control and an air by-pass adapter (which is simply a perforated length of plastic pipe). Both these are needed in order to vary the air flow rate through the porous bed;

(iii) a 3 mm stainless steel pitot-tube (Dwyer No. 166-6) to measure velocities from 0.05 to 15 m/s (10 to 3000 ft/min). Tables for different pipe diameters (as described in Ref. [4]) enabled the corresponding volume flow rate to be deduced;

(iv) an electric digital micromanometer (EDM) (Neotronics Model EDM-1) which can measure pressures with a resolution of 0.025 x 10^{-3}m (10^{-3} in.) of water or 0.25 Pa, and having a maximum range of up to 0.5 m (20 in.) of water. This is also described in Ref [4].

Other apparatus included two mounting devices: (i) a 0.038 m (1.5 in.) outer diameter brass pipe to connect the suction hole to the vacuum hose with arrangements to attach the pitot tube [called the Flow Pressure Tube (FPT)], and also the EDM, and, (ii) a 0.019 m (0.75 in.) stainless steel pipe to mount the EDM in order to measure the pressure at each of the nine different taps. These devices have already been described in detail in a previous report[4]. All measurements performed were in accordance with the approved QA project plan [22]. Certain details are given in Appendix C.

The experimental procedure for the apparatus filled with a certain type of porous medium entailed fixing the 0.038 m (1.5 in.) FPT device (inner diameter of 0.035 m or 1.36 in.) above the central suction hole of the top plywood disk and connecting it to the suction hose of the vacuum cleaner. A pressure tap at this pipe (see Fig. 7) placed 5 diameters above the suction hole permitted the static vacuum pressure to be measured as well, which could then be used to get an estimate of pressure losses due to changing direction and cross-section, and also due to turbulence at entry into the pipe.

An experimentation run consisted first of selecting a certain total air flow rate and gradually changing the speed of the vacuum cleaner in order to achieve this flow rate. The pressure measurements (representative of the corresponding static pressure inside the porous bed) at each of the nine taps were then taken in turn with all other taps closed. This completed a series of readings pertaining to one run. In subsequent runs, the total air flow rate was set to another predetermined value and the readings were repeated.

6. Experimental Results and Analysis of Radial Flow

Table 1 summarizes the different experiments performed using the laboratory apparatus. For example, Experiment A involved river-run gravel of nominal diameters of 0.012 and 0.019 m (1/2 in. and 3/4 in.) which we shall refer to as small and large gravel, respectively. Experiments A1 and A2 differ only in the spacing between the plywood disks, i.e., the thickness of the gravel bed was altered. Experiment A1 involved three separate runs each with a different total volume flow rate, the specific values of which are also given in Table 1. The flow regime (based on the corresponding Reynolds number) was found to be turbulent throughout the radial disk.

The specific values of the mean gravel diameter and the porosity of the bed are required for computing the Reynolds number [given by eq.(1)]. We have performed porosity measurements and also computed the mean equivalent diameter of the various porous bed materials chosen in the present study; these are described in detail in Appendix B.

Also, in all the analyses involving regressions which are discussed below, the values of the static pressure at hole 10 were not included since it is very likely that the turbulence due to entrance effects would still be present that close to the outer periphery of the disk.

Table 1. Summary of the different experiments performed with the laboratory apparatus using river-run gravel

Experiment	Gravel size (nominal diameter)	Disk spacing	No. of runs	Total flow rate (cfm)	Total flow rate l/s
A1	1/2 in. (0.012 m)	3 in. (0.075 m)	3	43.5	20.5
				63.8	30.1
				79.0	37.3
A2	1/2 in. (0.012 m)	3.75in. (0.10 m)	2	46.8	22.1
				66.5	31.4
A3	3/4 in. (0.019 m)	3.75in. (0.10 m)	4	23.7	11.2
				32.2	15.2
				37.4	17.6
				44.0	20.8

Table 2. Results of regression using a quadratic model for pressure drop [eq.(11)]

Experimental run	No. of data points	R^2 Model without intercept	R^2 Model with intercept	Parameter 'a' Mean	Parameter 'a' SEM
A1	24	0.964	-	344.7	13.82
A2	16	0.975	-	358.2	14.84
A1+A2	40	0.968	0.953	350.1	10.13
A3	28	0.967	0.914	303.4	10.72

From Table 1, we note that the flow is likely to be turbulent. Hence we start by regressing the observed data following eq.(11). Table 2 assembles the subsequent results. Since caution is recommended when the soundness of a regression model is to be judged according to its coefficient of determination (i.e. the R^2 value) [23], we have also run the model with an intercept and found no appreciable discord between the two sets of R^2 values (see Table 2). Consequently, in our present study, we can assume the R^2 value to be indicative of the goodness-of-fit of the no-intercept model. We also note from Table 2 that the estimated values of the constant 'a' differ only by about 5%. This is how one would expect it to be since permeability of the bed (inversely related to the coefficient 'a' as given by eq.(4)) should not alter with change in the thickness of the porous bed. This suggests that the foam attached to the top plywood disk of our laboratory apparatus does seem to do a satisfactory job of eliminating short-circuiting of air flow. In order to get average estimates, we have treated the observations of Exps.A1 and A2 together and estimate the 'mean' parameters. The corresponding value is also shown in Table 2. In general, the Standard Error of the Mean (SEM) values are 5% or less of the mean value, a gratifying observation.

We note that R^2 values are very high despite which, as depicted by Figs. 10 and 11, the fits could be improved. Consequently, we have rerun the regression using eq.(9) wherein both the constant 'a' and the exponent 'b' are to be determined by least square errors. Instead of simply determining the optimal value of the exponent b we have performed several runs the results of which are summarized in Table 3. Such an approach yields insight into the sensitivity of the parameters a and b on the regression. We note that R^2 values have improved significantly and one cannot realistically expect better fits (given the measurement errors in our readings, we may in fact be overfitting in the sense that we are trying to assign physical meaning to random errors), as compared to assuming a quadratic exponent (see Table 2). This is also seen in Figs. 12 and 13 where we note

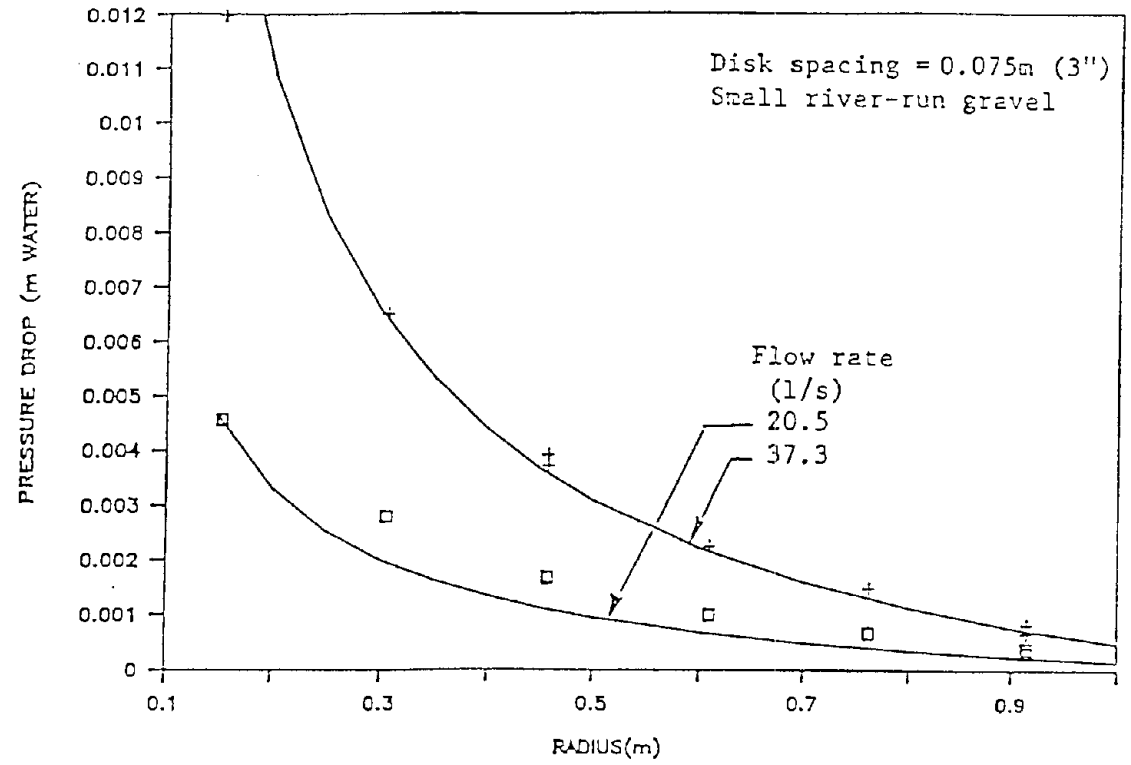

Fig. 10 Data from Exps. A1 and A2 versus model with exponent b = 2 (eq. (11)).

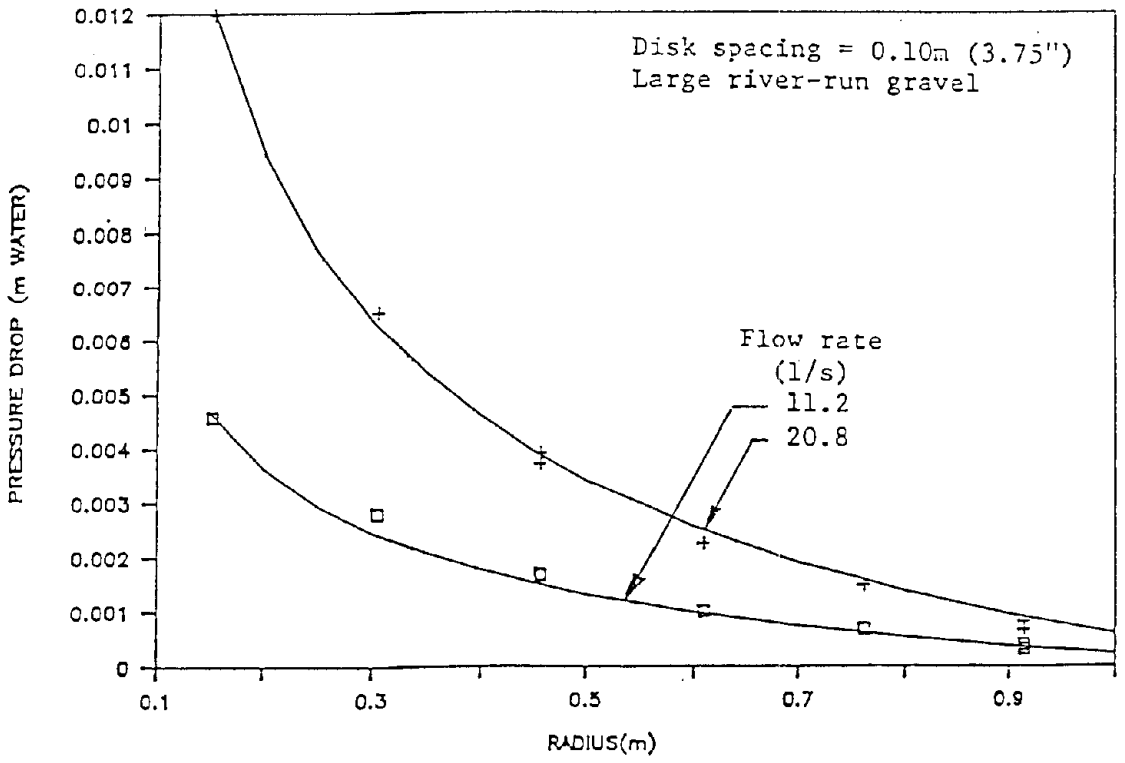

Fig. 11 Data from Exp. A3 versus model with exponent b = 2 (eq. (11)).

Table 3. Results of regression using an exponential model for pressure drop [eq.(9)]. The underlined values of b correspond to those yielding the highest R^2.

Experimental run	No. of data points	b	R^2	Parameter 'a' Mean	Parameter 'a' SEM	Effective permeability of porous bed (m^2)
A1+A2	40	1.3	0.984	86.71	1.78	
		1.4	0.991	106.8	1.59	
		1.5	0.996	130.6	1.30	
		<u>1.6</u>	0.998	158.5	1.15	9.4×10^{-9}
		1.7	0.997	191.2	1.75	
A3	28	1.2	0.994	23.60	0.34	
		1.3	0.996	32.35	0.39	
		<u>1.4</u>	0.997	44.22	0.50	34×10^{-9}
		1.5	0.996	60.26	0.74	
		1.6	0.994	81.90	1.22	

Table 4. Results of regressing experimental data from House 21 using eq.(10)

Trial run	b	k (m^2)	SEM (%)	R^2	Remarks
1	1.6	9.3×10^{-9}	6-7	0.80	With all data points
	1.7	7.5×10^{-9}		0.80	
2	1.6	7.1×10^{-9}	3	0.96	With data of holes 11 and 12 removed
	1.7	5.8×10^{-9}		0.97	
3	1.6	10.0×10^{-9}	5	0.88	With data of holes 9, 10, 11, and 12 removed
	1.7	7.3×10^{-9}		0.87	

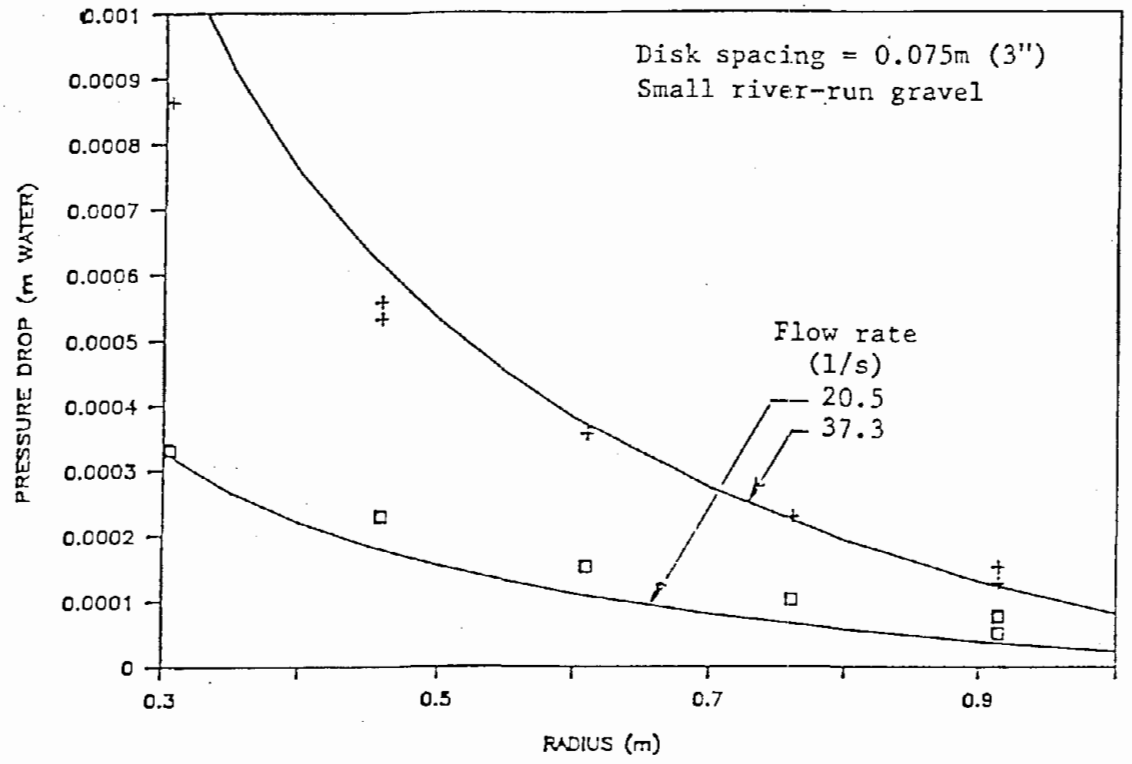

Fig. 12 Data from Exps. A1 and A2 versus model with exponent b = 1.6 (eq. (9)).

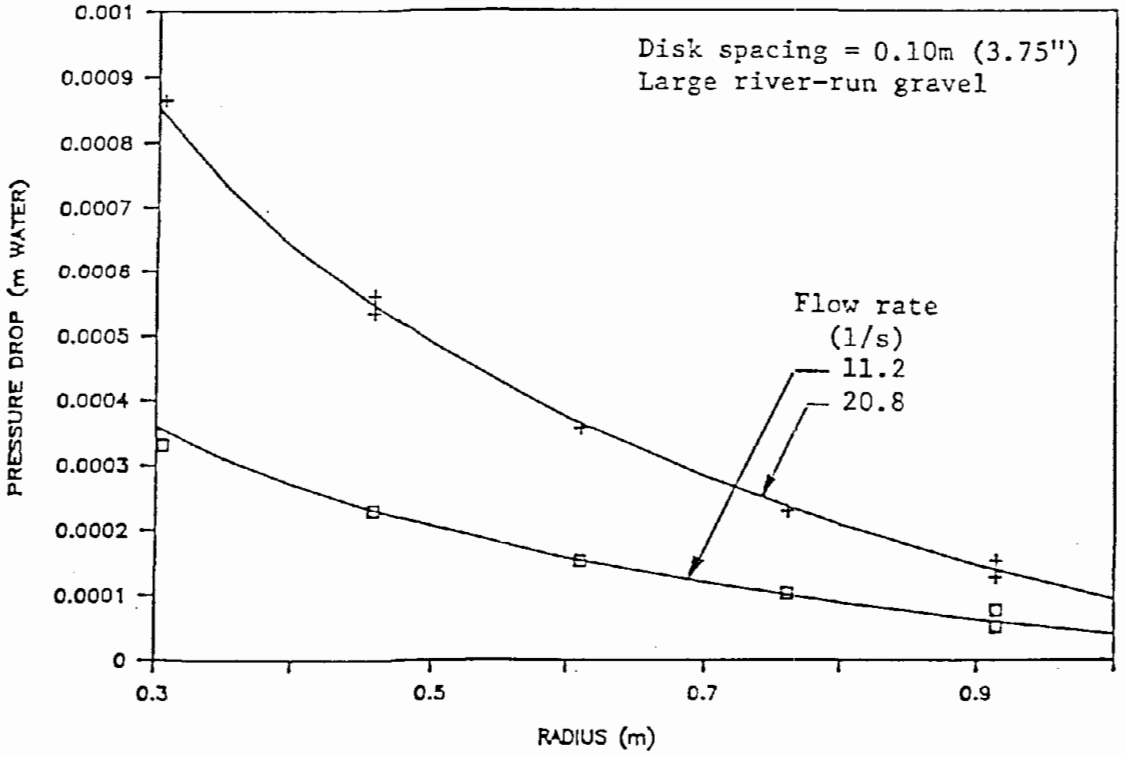

Fig. 13 Data from Exp. A3 versus model with exponent b = 1.4 (eq. (9)).

that the fit between model predictions and observed pressure drop has improved.

The value of the exponent b that yields the highest R^2 value is underlined in Table 3. Note also that the SEM values for the estimate of 'a' are relatively small.

Other aspects need specific mention as well:

(a) We find that for the type of river run gravel used and for the range of flow conditions investigated, the effect of pressure drop in the flow arising as a result of changing cross-sectioned area [i.e. the second term on the RHS of eq.(9)] corresponds to less than a percent of the total pressure drop. Thus eq.(10) is the appropriate one to use in order to predict pressure fields in porous gravel beds under flow conditions akin to those encountered during operation of practical radon mitigation systems.

(b) We note that the optimal value of b is not too well determined, since R^2 values only change in the third decimal point when b is varied in steps of 0.10 (Table 3). It is highly unlikely that the experimental accuracy of our readings can lead us to place this much faith in the exact or best value of b identified by regression. Consequently, one should rather think in terms of a certain range for the b values and not try to attach undue importance to physical interpretation of the exact value of the exponent b.

(c) The study referred to earlier [8] found values of the exponent b to be 1.56 for the cylindrical disk model. This is generally bourne out in the present study where we find b=1.6 for the small river-run gravel and b=1.4 for the large gravel.

(d) There is however a serious drawback in our ability to accurately determine the values of the bed permeabilities from the present experiments. This is because the present data were collected during turbulent flow regimes, and though the estimate of parameters a and b identified by regression are perfectly satisfactory for predicting pressure drops at flow regimes in the range within which the present experiments

were performed, these estimates may yield misleading and erroneous predictions when used outside this range of flow conditions. In other words, parameter sets identified by regression are not generally accurate for extrapolation purposes.

In order to make this point clearer, let us rewrite eq.(10) as follows:

$$\ln\left(-\frac{p(r)-p_a}{\rho_w.g}\right) = \ln\left(\frac{1}{k}\cdot\frac{\nu_a}{g}\right) + \ln\left[-\frac{\rho_a}{\rho_w}\cdot\left(\frac{q}{2\pi h}\right)^b\cdot\frac{1}{(1-b)}\cdot(r^{1-b}-r_o^{1-b})\right] \qquad (15)$$

If we were to plot the term on the left-hand side on the y-axis and the second term on the right-hand side of the above equation on the x-axis, the intercept of such a line would give us an estimate of the permeability. Figure 14 shows such a representation for the experimental data using small gravel (Experiments A1 and A2) and b=1.6. It is now clear that since the data points essentially lie in a region far away from the x-axis, the intercept term is bound to be ill-defined from a subsequent statistical regression. The values of effective permeability of the porous bed calculated following eq.(4) are included in Table 3 and show a three fold difference between small and large gravel sizes. The numerical values do seem to correspond to those cited in the radon literature [9, 24]. If more accurate values of permeability are to be determined, the experimental design of our apparatus needs to be suitably modified.

There is another purely statistical limitation in identifying parameters from a least square regression such as the present, where a mathematical model without an intercept term is fitted to quantities which vary drastically like the pressure drop quantities do as one moves radially outward (Figs. 10-13 indicate an order of magnitude variation). The regression would favor the larger values of pressure drop since it tries to capture as much of the variation in observed values of pressure drop in terms of absolute variation from zero. Consequently the model parameters estimated will not be very sound because the

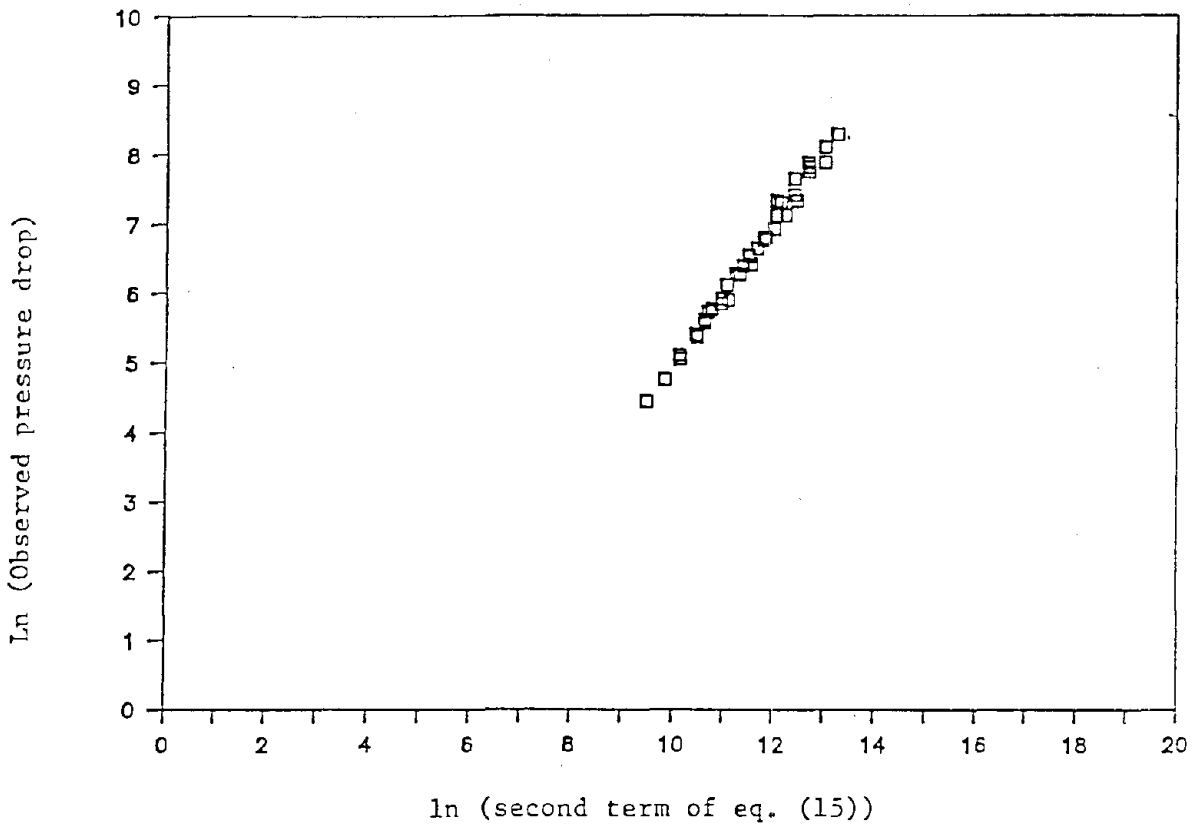

Fig. 14 Log-log plot of the observed pressure drop values of Exps. 1 and 2, in meters of water, versus those of the second term on the left hand side of eq. (15). This figure serves to illustrate the fact that the intercept, which corresponds to the permeability of the porous bed, cannot be estimated very accurately from regression of the data points at hand.

regression is unduly influenced by a relatively small number of observations. One possibility is not to evaluate goodness-of-fit between model and observed data based on the R^2 statistic but rather on the Chi-square statistic [23]. Though this test would overcome the above mentioned limitation, other problems (beyond the scope of this report) are likely to arise. Another possibility could involve performing more measurements at higher pressure drops in order to avoid such uncertainty in the estimated parameters. These issues will have to be addressed in subsequent studies.

7. Field Verification

The irregular boundary conditions and the non-homogeneity in subslab beds that arise in practice are however not easily tractable with a simple expression such as eqs. (10) and (13), and resorting to a numerical computer code may be the only rigorous way to proceed in order to predict pressure fields under actual situations [7,14]. We shall show in this section that our simplified approach nevertheless has practical relevance in that it could be used as a means of determining which areas under the slab have poorer connectivity as compared to the rest.

The house under investigation (H21) has a partial basement with a gravel bed under the basement slab. As shown in Fig. 15, the basement (though rectangular) is close to being square (6.45m x 7.60m). It has two sides exposed to the ambient air above grade, while the other two sides are adjacent to slab-on-grade construction. The 0.1m suction hole is situated roughly at the center of the basement slab. Though 19 holes were drilled across the slab, (Fig. 15), two of them (holes 11 and 12) were found to be blocked beneath the slab. Consequently, pressure data measured by the EDM from only 17 holes have been used in this study. This blockage was later found to be due to the presence of an oversized footer for a support column.

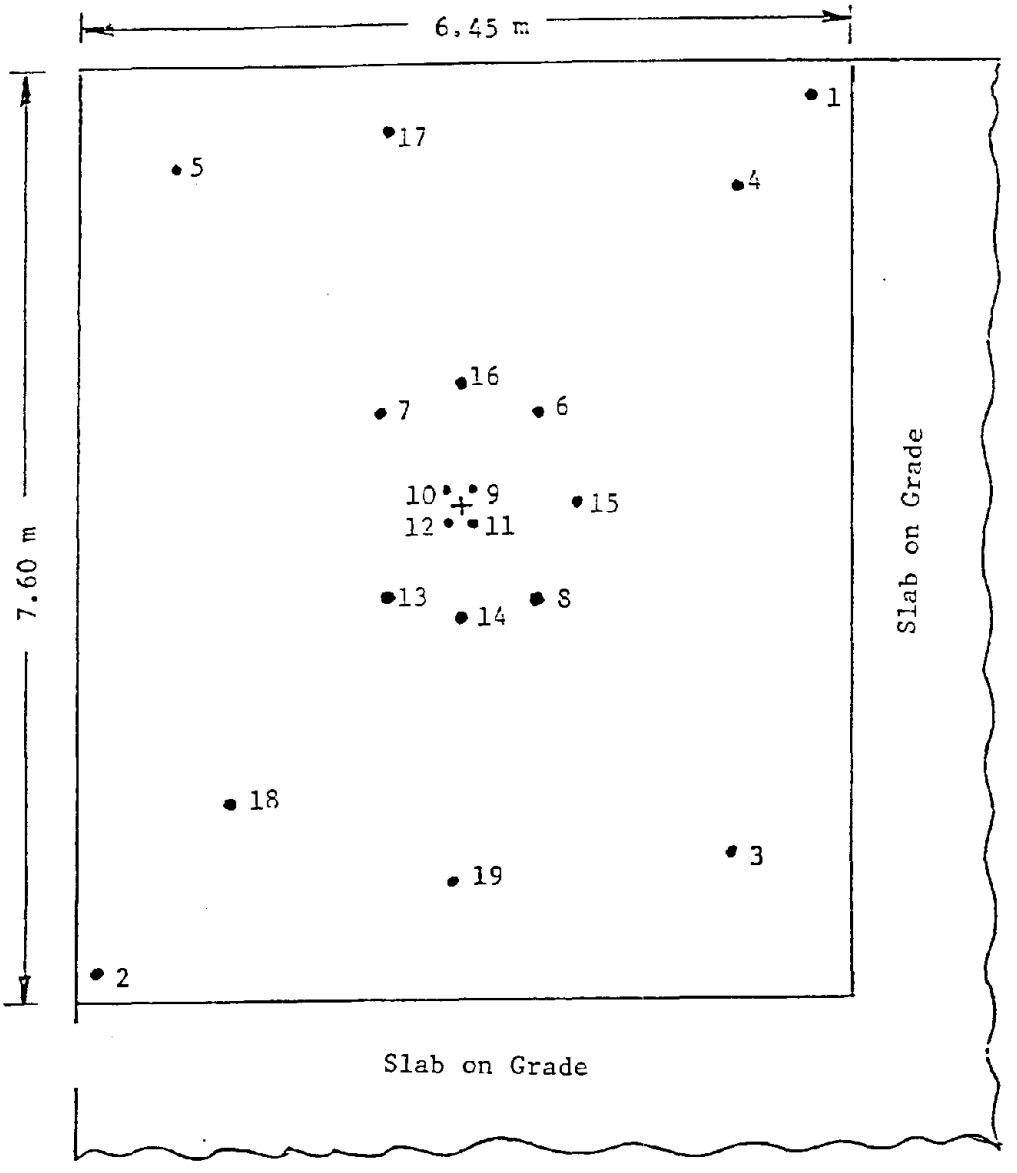

Fig. 15 Plan of the basement of House 21 showing the relative positions of the various subslab penetrations. The suction hole of the mitigation system is marked as a +.

All measurements performed in this house were in accordance with the approved QA/PP project plan [22]. Certain details are given in Appendix C. Three sets of runs were carried out which we have termed as follows depending on the air flow rate through the FPT device described earlier:

(i) 28 L/s - High flow,

(ii) 23.4 L/s - Medium flow

(iii) 18.1 L/s - Low flow

Note that our analytical expression for the pressure field under turbulent flow given by eq. (10) is strictly valid for a circular disk with the boundary conditions being that at $r = r_o$, $p = p_a$. We approximate the rectangular basement by a circle of 3.5m mean radius. We need to also include the extra path length of ambient air flowing down the outer basement wall, going under the footer, and then flowing through the subslab gravel into the suction hole. We estimate this to be about 2m. Consequently, we find $r_o = 5.5$m. The thickness of the subslab gravel bed h has been found to be about 5cm.

The gravel under the slab, though river-run, were found to be highly heterogeneous in size and shape. In general, their average size was slightly less than 0.012m. However, we decided to use the properties of the 0.012m gravel determined experimentally in the laboratory (See Table 1).

Figure 16 shows the observed and calculated pressure drops for the high and low flow rates. Readings from holes 13 and 14 are lower and we suspect poorer connectivity to these holes, i.e., some sort of blockage in this general area. We note that the agreement between model and observation is indeed striking given the simplification in our model and also the various assumptions outlined above.

The previous figures indicate which areas under the slab are non-uniform. A better way of illustrating how well the model fares against actual observations is shown in Fig. 17. The solid line represents the model predictions while observations are shown by

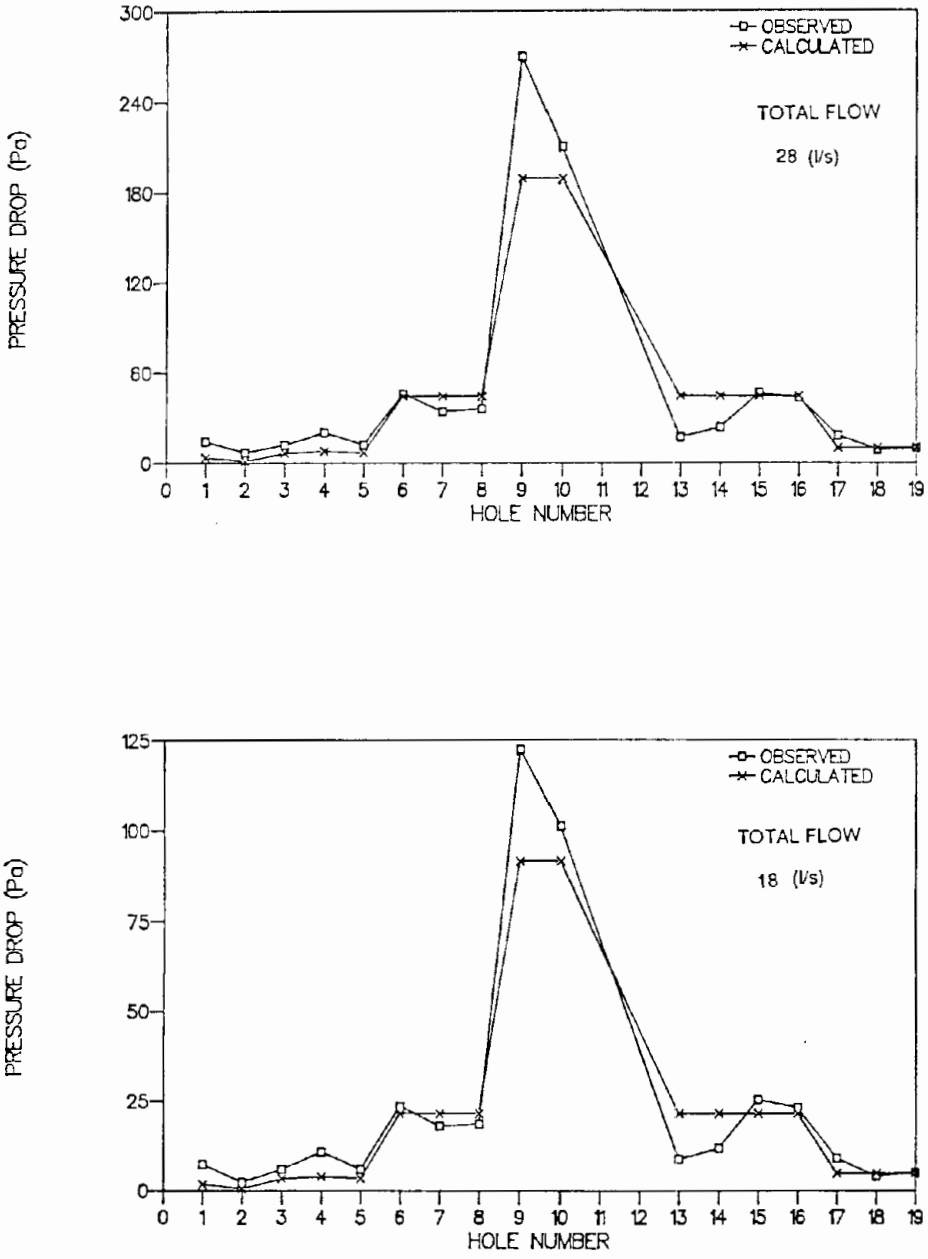

Fig. 16 Comparison of observed and computed pressure drops for different subslab penetrations using coefficients of 0.012 m gravel ($b = 1.6$ and $k = 9.4 \times 10^{-9}$ m^2). Data of hole 12 not included.

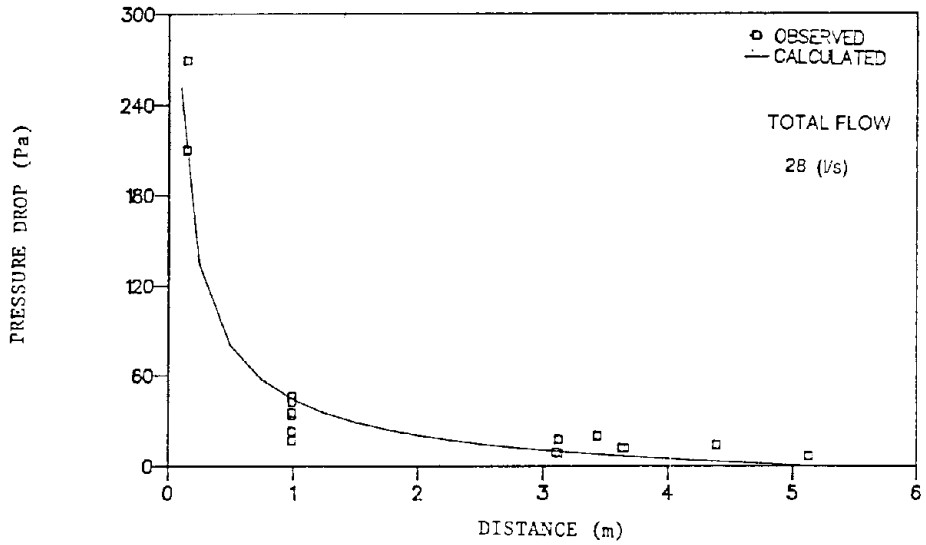

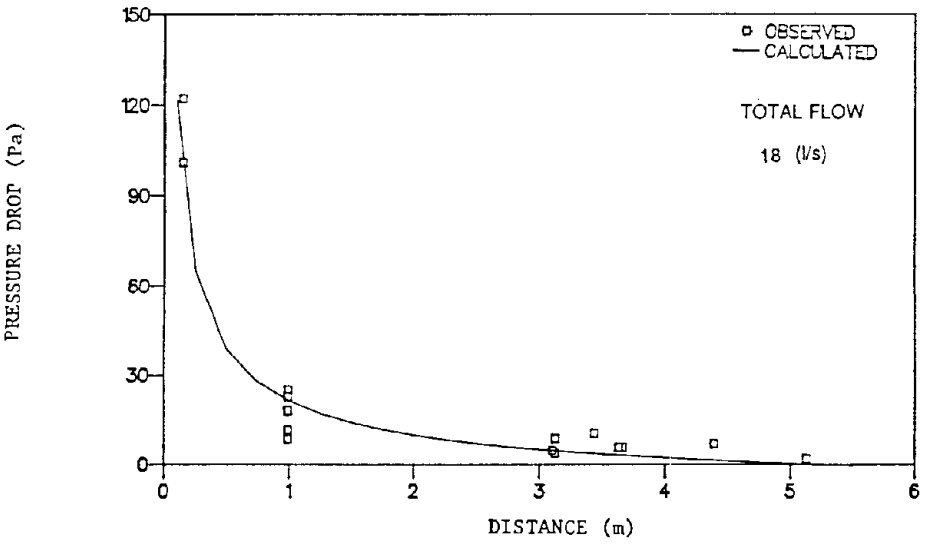

Fig. 17 Same as Fig. 16 but with distance from suction hole.

discrete points. We note again the satisfactory predictive ability of this modeling approach and also the fact that certain holes have pressure drop values higher than those predicted by the model.

In order to illustrate the fact that our approach is sensitive to the selection of type of gravel bed, Fig. 18 presents the experimental observations plotted against model predictions with gravel bed coefficients taken to be those that correspond to the 0.019m gravel. We note the very large differences between model prediction and observed pressures over the entire basement, thereby suggesting that our approach has enough sensitivity to be of practical relevance.

An alternate approach to the one adopted here and described above, would be not to assume specific gravel bed coefficients but to determine these from regression. This entails using eq.(10) along with the data set of actual observations and determining the parameters k and b by regression. Since b is not a parameter that varies greatly [8], we have chosen two different values of b (1.6 and 1.7) to see what difference this leads to in terms of the coefficient of determination (R^2) and in the values of k.

Regression results are summarized in Table 4. We have performed three different trial runs. The first uses all data points. In trial 2, pressure drop observations from hole 12 (hole that is blocked) have been removed. We note that the R^2 improves dramatically, from 0.80 to 0.96. For trial run 3, holes 9, 10, and 12 have been removed in order not to bias the regression since these holes have high pressure drop values. We note that the R^2 of trial run 3 is 0.88, an improvement over that of trial 1.

Other than the very high R^2 values found, the most striking feature is that regression yields a value of k which is practically identical to that of the 0.012m gravel determined experimentally in our laboratory apparatus. This suggests that even a visual inspection

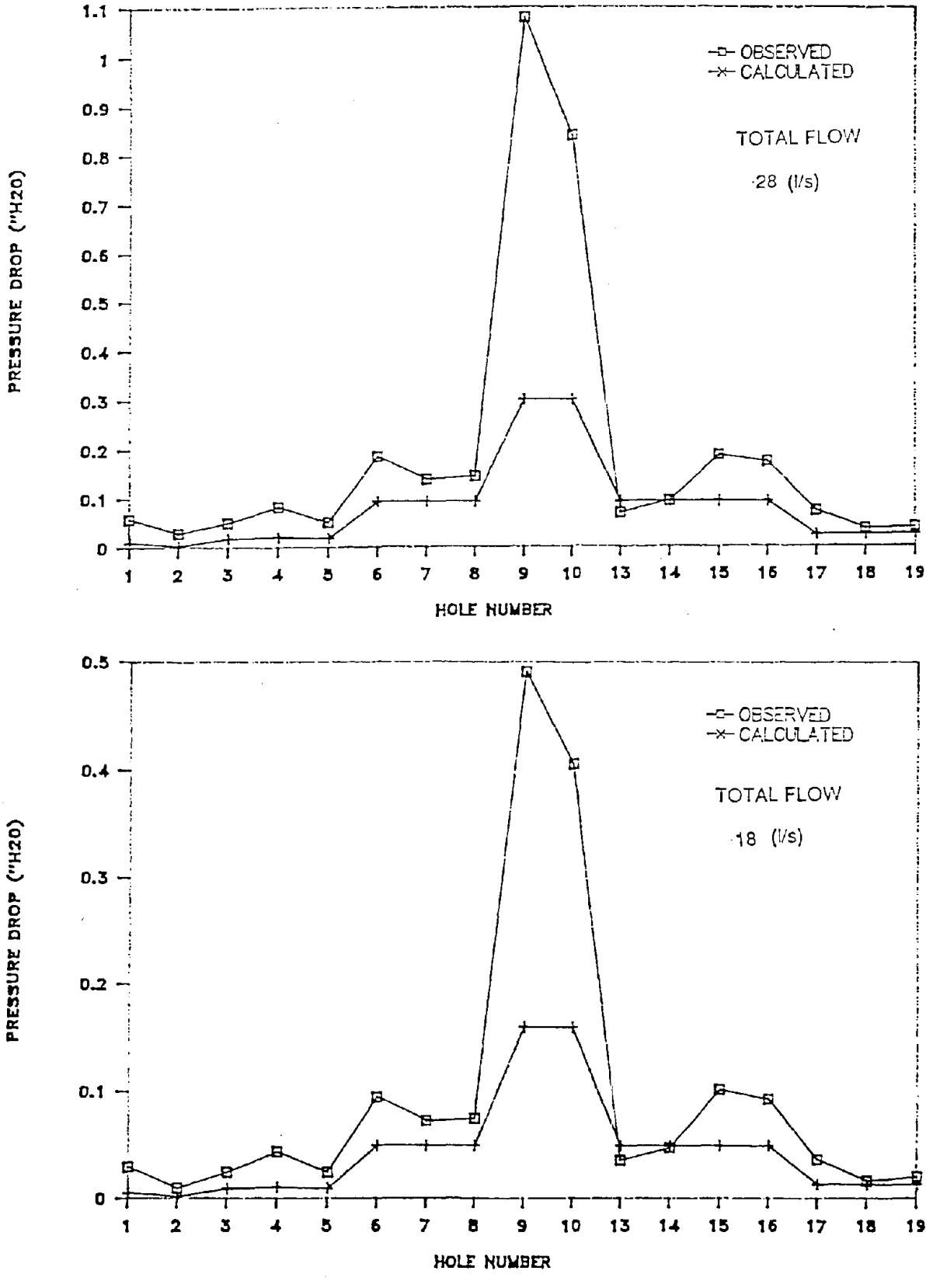

Fig. 18 Same as Fig. 16 but using coefficients of 0.019 m gravel (b=1.4 and $k=3.4 \times 10^{-9}$ m^2).

of the porous material under the slab can be an indicator good enough for a mitigator to select a standard bed material and using the physical properties of the material get a sound estimate of what the suction pressure ought to be in order to generate a certain pressure field under the slab. The need to categorize commonly found subslab material, deduce their aerodynamic pressure drop coefficients in laboratory experiments, and thence tabulate these in handbooks seems to be worth investigating.

8. Graphical Representation

The approach developed here will serve to illustrate how closed form solutions for the pressure drop in porous beds can be represented in graphical form suitable for professional radon mitigators. Let us illustrate our approach using the simplest case of a circular porous bed with radial inflow between two impermeable disks. From the discussion in the above section, it would seem that we could equally apply our model to square basements and also to houses with a partial basement.

Equation (13) is valid for laminar flow which would prevail where soil is the subslab material. It can be written as:

$$\Delta p_h(r) \cdot k = (\nu_a/g) \cdot (\rho_a/\rho_w) \cdot (1/2\pi) \cdot (q/h) \cdot \ln(r/r_o) \qquad (16)$$

where Δp_h is the pressure drop in head of water and is equal to $[p(r)-p_a]/(\rho_w \cdot g)$.

Four curves have been plotted in Fig. 19 for four different values of (q/h): $1.0 \cdot 10^{-3}$ m²/s, $5 \cdot 10^{-3}$ m²/s, $1 \cdot 10^{-2}$ m²/s, $2 \cdot 10^{-2}$ m²/s. Thus, if the values of (r/r_o), (q/h), and k are known, $\Delta p_h(r)$ can be obtained from this graph.

In the case of gravel under the slab, the flows will probably be turbulent and the pressure drop is given by eq. (10) which can be rewritten as:

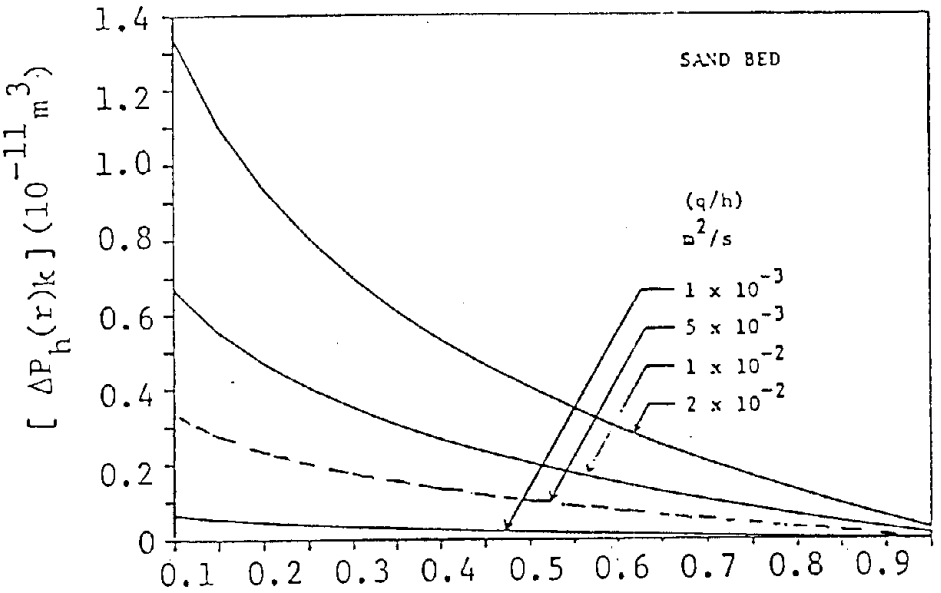

Fig. 19 Pressure drop in a sand bed with radial airflow between two impermeable disks.

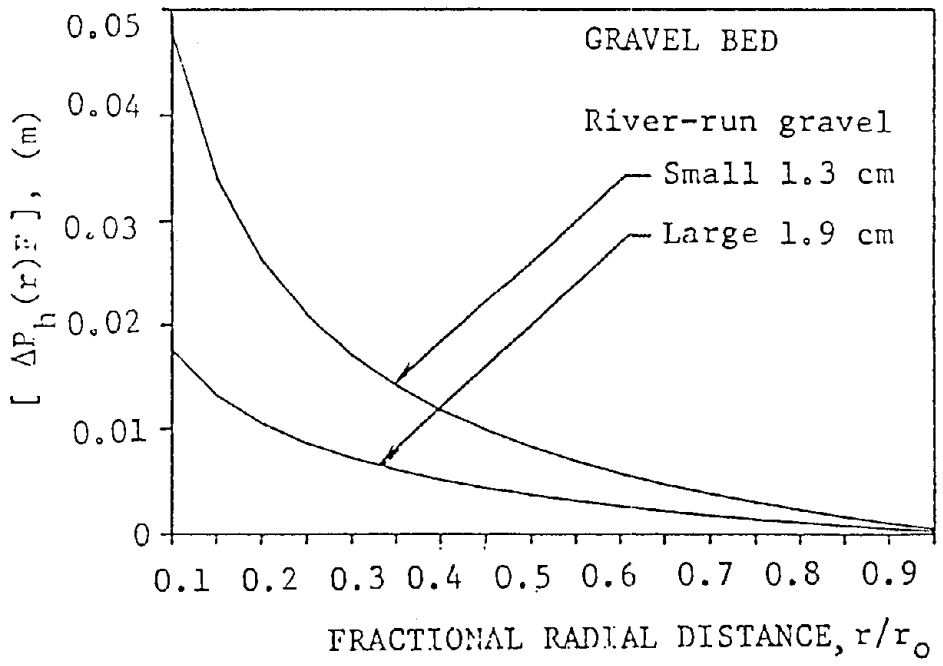

Fig. 20 Pressure drop in a gravel bed with radial airflow between two impermeable disks. The correction factor F can be determined from Fig. 21.

$$\Delta p_h(r) \cdot F = (1/k) \cdot (\nu_a/g) \cdot (\rho_a/\rho_w) \cdot [(1/2\pi)^b)] \cdot [1/(1-b)] \cdot [(r/r_o)^{1-b}-1] \quad (17a)$$

$$\text{where } F = [(r_o^{(1-b)}) \cdot (q/h)^b]^{-1} \quad (17b)$$

Figure 20 shows plots for $(\Delta p_h(r) \cdot F)$ vs. (r/r_o). Two curves have been plotted for the two different values of b and k. Figures 21a, 21b, and 21c show plots for the correction factor F for different values of r_o and (q/h) values of 0.05 m^2/s, 0.5 m^2/s, and 7.5 m^2/s. Each graph has two curves, each representing a different value of b (1.4 or 1.6). It is easily seen that these graphs can be utilized to obtain values for $\Delta p_h(r)$ for given values of r, r_o, and q/h.

Figures 19, 20, and 21 have been presented here in order to illustrate how, from a closed-form equation, figures can be generated which would be useful to practitioners. The figures are not meant to cover the entire gamut of conditions which may arise in actual practice.

9. Pressure Drop Considerations

There are basically three different sources of pressure drops in the mitigation system.

$$\Delta p_{total} = \Delta p_{bed} + \Delta p_{ent} + \Delta p_{pipe} \quad (18)$$

where Δp_{bed} = pressure drop in porous bed,

Δp_{ent} = pressure drop due to change of direction and that associated with entrance effects into the mitigation pipe,

Δp_{pipe} = pressure drop in the mitigation pipe.

The pressure drop in the subslab bed is given by equations akin to eqs. (10) or (13). The pressure drop at the entrance to the suction pipe involves accounting for the following effects; (i) change in flow direction, (ii) change in cross-sectional area, (iii) entrance effects

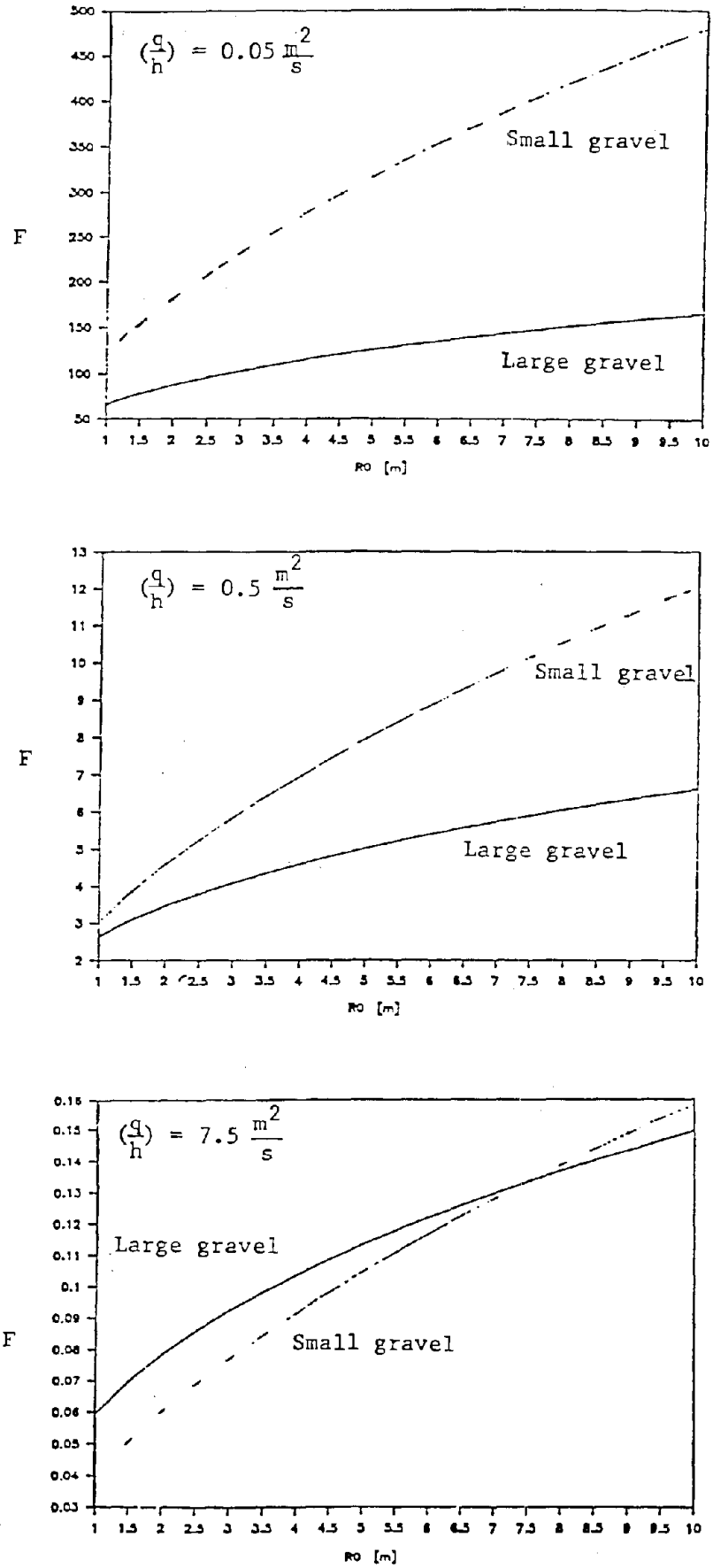

Fig. 21 Correction factor F for gravel beds to be used in Fig. 20.

at the throat of the suction pipe. From an engineering viewpoint, it is more convenient to treat these together. In accordance with actual practice [25], we propose the following simplified empirical equation for the head loss:

$$(\Delta p_{ent}/\rho_w \cdot g) = K_p \cdot [1-(A_p/A_b)]^2 \cdot (V_p^2/2g) \quad (19)$$

where K_p is the dimensionless pressure loss coefficient which should not depend on the velocity or the bed thickness, and is a constant for a specific type of bed material,

A_p is the cross-sectional area of the suction pipe,

A_b is the surface area of a cylinder of diameter equal to that of the suction pipe and height equal to the thickness of the porous bed, and

V_p is the velocity of air in the suction pipe.

If d_p is the diameter of the suction pipe, then:

$$A_p/A_b = (\pi d_p^2/4) \cdot (1/\pi d_p h) = (d_p/4h) \quad (20a)$$

and

$$V_p = q/A_p = 4q/\pi d_p^2 \quad (20b)$$

Table 5 assembles the results of determining the entry pressure loss coefficient for three different flow rates. We note that K_p values are exactly the same, a gratifying result. This enables us to place a certain amount of confidence in our model for the entrance losses.

The pressure drop in the piping includes losses due to elbows, fittings, as well as straight pipe. Following Ref. [25], losses in the straight pipe is given by:

$$\Delta p_{pipe} = f \cdot (L/d_p) \cdot (q/A)^2/2g \quad (21)$$

Table 5. Determination of the pressure loss coefficient at the throat of the mitigation suction pipe in House 21

Run	Total Air flow (L/s)	Suction pressure before entry (cm water)	Suction pressure after entry (cm water)	K_p
1	18.3	1.300	1.664	0.053
2	23.4	1.938	2.540	0.053
3	28.4	2.700	3.589	0.053

Table 6. Relative pressure drops in the mitigation system of House 21

Run	Total Air flow (L/s)	Δp_{bed} (cm water)	Δp_{ent} (cm water)	Δp_{pipe} (cm Water)	Hydrodynamic effectiveness (%)
1	18.3	1.30	0.363	8.0×10^{-3}	77.8
2	23.4	1.94	0.602	13.0×10^{-3}	75.9
3	28.4	2.70	0.889	17.7×10^{-3}	74.9

Pressure losses in bends and fittings are normally expressed in terms of an equivalent pipe diameter. For example, a 90° elbow has the same pressure drop as a straight pipe of length equal to about 25 times the pipe diameter [25].

Since the primary objective of the mitigation system is to create a suction pressure under the slab only, we can define a hydrodynamic effectiveness of the mitigation system based on these three pressure drops.

$$\text{Hydrodynamic effectiveness} = \Delta p_{bed} \; / \; \Delta p_{total} \tag{22}$$

We have computed these various pressure drop values for the case of H21 in order to get an idea of the relative magnitude of these pressure drops. The mitigation system (with one suction hole only) in H21 has about 7m of straight pipe of 0.1m diameter and three 90° elbows. This translates into a total length of (7+3·25·0.1) = 14.5 m.

Table 6 assembles the various pressure drops in the three elements of the mitigation system. While Δp_{bed} and Δp_{ent} have been measured, Δp_{pipe} has been calculated from eq. (21). The hydrodynamic effectiveness defined by eq. (22) is also given.

We note from Table 6 that Δp_{pipe} is negligible compared to Δp_{bed}, while Δp_{ent} is about 30% of Δp_{bed}. The hydrodynamic effectiveness is close to being independent of the flow rate and is about 75%. Thus 75% of the energy used up by the suction fan goes directly into creating the subslab depressurization while the rest can be regarded as being redundant expenditure of energy. Though present knowledge does not permit us to suggest a particular value for the optimal hydrodynamic effectiveness, we suggest that future engineering guidelines dealing with mitigation system design specify a working range for this index.

10. Future Work

Logical extensions of this study would involve applications of this methodology to houses with (i) homogeneous beds but with irregular boundaries, and (ii) non-homogeneous porous beds. One approach is to develop a computer program using numerical methods (either finite element or finite difference could be used) to solve the basic set of hydrodynamic and mass conservation equations [7,14]. Pressure fields under the slab for practically any configuration could be thereby predicted. An optimization algorithm could then be attached to the above program in order to obtain the optimal layout and the number of mitigation suction points for the particular subslab conditions such that certain well-defined and physically relevant constraints are satisfied.

Our present line of thinking is that though the above approach offers great flexibility, it is not easy to use by non-experts. Developing engineering guidelines for practitioners based on such a code demands a certain amount of effort and practical acumen. It would be wiser to define a few "standard" cases of basement shape, subslab conditions and mitigation pipe locations; try to develop simplified closed-form solutions of these cases; and then see how well these solutions fare with respect to actual measurements taken in the field. If such an approach does give satisfactory engineering accuracy, its subsequent use to mitigation system design would be relatively simple and straightforward.

References

1. D.T. Harrje and L.M. Hubbard, Proceedings of the Radon Diagnostics Workshop, April 13-14, 1987, EPA-600/9-89-057 (NTIS PB89-207898), June 1989.

2. J. Wang and M. Cahill, Radon reduction efforts in New Jersey, presented at the Annual Meeting of the National Health Physics Society, Boston, MA, July 4-8, 1988.

3. D.C. Sanchez, Technical issues related to emission releases from subslab radon mitigation systems, presented at ASCE National Conference on Environmental Engineering, Austin, TX, July 9-12, 1989.

4. K.J. Gadsby, L.M. Hubbard, D.T. Harrje, and D.C. Sanchez, Rapid Diagnostics: Subslab and Wall Depressurization Systems for Control of Indoor Radon, in Proceedings: the 1988 Symposium on Radon and Radon Reduction Technology, Volume 2, EPA-600/9-89-006b (NTIS PB89-167498), March 1989.

5. B. H. Turk, J. Harrison, R. J. Prill, and R. G. Sextro, Soil gas and radon entry potentials for substructure surfaces, in Proceedings: the 1990 International Symposium on Radon and Radon Reduction Technology, Volume 2, EPA-600/9-91-026b (PB91-234450), July 1991.

6. C.S. Fowler, A.D. Williamson, B.E. Pyle, F.E. Belzer, and R.N. Coker, Engineering Design Criteria for Sub-Slab Depressurization Systems in Low-Permeability Soils, EPA-600/8-90-063 (NTIS PB90-257767), August 1990.

7. J.M. Barbar and D.E. Hintenlang, Computer Modeling of Subslab Ventilation Systems in Florida, 34th Annual Meeting of Health Physics, Abstract No. TAM-E8, Albuquerque, NM, 1989.

8. T.G. Matthews, D.L. Wilson, P.K. TerKonda, R.J. Saultz, G. Goolsby, S.E. Burns, and J.W. Haas, Radon diagnostics: subslab communication and permeability measurements, in Proceedings: the 1988 Symposium on Radon and Radon Reduction Technology, Volume 1, EPA-600/9-89-006a (NTIS PB89-167480), March 1989.

9. W.W. Nazaroff, B.A. Moed, and R.G. Sextro, 'Soil as a source of indoor radon generation, mitigation and entry,' Chap.2, Radon and Its Decay Products in Indoor Air, W.W. Nazaroff and A.V. Nero (Eds.), John Wiley and Sons, NY 1988.

10. A.G. Scott, 'Preventing radon entry,' Chap.10, Radon and Its Decay Products in Indoor Air, W.W. Nazaroff and A.V. Nero (Eds.), John Wiley and Sons, NY 1988.

11 R.C. Bruno, Sources of indoor radon in houses, J. Air Pollution Control Association, Vol.33, pp.105-109, 1983.

12. W.W. Nazroff, B.A. Moed, R.G. Sextro, K.L. Revson, and A.V. Nero, 'Factors Influencing Soil as a Source of Indoor Radon: A Framework for Geographically Assessing Radon Source Potentials,' report LBL-20645, Lawrence Berkeley Laboratory, Berkeley, CA 1985.

13. R.J. Mowris, 'Analytical and Numerical Models for Estimating the Effect of Exhaust Ventilation on Radon Entry in Houses with Basements or Crawl Spaces,' M.S. Thesis, Lawrence Berkeley Laboratory, Berkeley, CA 1986.

14. C. de Oliveira Loureiro, 'Simulation of the Steady-state Transport of Radon from Soil into Houses with Basement under Constant Negative Pressure,' LBL-24378, Lawrence Berkeley Laboratory, Berkeley, CA 1987.

15. V.C. Rogers and K.K. Nielson, Benchmark and application of the RAETRAD model, in Proceedings: the 1990 International Symposium on Radon and Radon Reduction Technology, Volume 2, EPA-600/9-91-026b, July 1991.

16. M. Muskat, The Flow of Homogeneous Fluids through Porous Media, McGraw-Hill, 1937.

17. R.E. Collins, Flow of Fluids Through Porous Materials, Reinhold Publishing Co., 1961.

18. A.E. Scheidegger, The Physics of Flow Through Porous Media, Univ. of Toronto Press, 3rd Edition, 1974.

19. P.S. Huyakorn and G.F. Pinder, Computational Methods in Subsurface Flow, Academic Press, 1983.

20. J. Bear, Dynamics of Fluids in Porous Media, Dover Publications, New York 1988.

21. J.D. Gabor and J.S.M. Boterill, 'Heat Transfer in Fluidized and Packed Beds,' Chap.6, Handbook of Heat Transfer Applications, W.M. Roshenow, J.P. Hartnett, and E.N. Ganic (Eds.), 2nd Edition, McGraw-Hill,1973.

22. C.S. Dudney, et al., Investigation of Radon Entry and Effectiveness of Mitigation Measures in Seven Houses in New Jersey, EPA-600/7-90-016 (NTIS DE89016676), August 1990.

23. G.E.P. Box, W.G. Hunter, and J.S. Hunter, Statistics for Experimenters: An Introduction to Design, Data Analysis and Model Building, John Wiley & Sons, New York 1978.

24. P.K. Hopke (Ed.), Radon and Its Decay Products, American Chemical Society, 1987.

25. ASHRAE, Handbook of Fundamentals, American Society of Heating, Refrigeration and Air-Conditioning Engineers, Atlanta, 1985.

Appendix A: Brief Review of Scientific Theory Relating to Flow through Porous Media [16-21]

A porous medium is defined as a solid containing holes or voids, either connected or unconnected, dispersed within it in either a regular or random manner such that holes occur relatively frequently within the solid [17]. In this study, we are specifically interested in unconsolidated isotropic beds such as sand or gravel and our discussion will be limited to such material. Since the structure of such beds is so irregular and random that it can be described only in statistical terms, the prevalent approach is to treat such beds on a macroscopic basis, analogous to the approach followed in the kinetic theory of gases. Thus, on a macroscopic scale the system can be defined in terms of a few determinable quantities from which phenomena like fluid flow or heat transfer can be accurately predicted for engineering purposes.

A1. Definitions of geometrical quantities

All the following properties are bulk properties in that they pertain to a unit total volume of the bed. Note that as such they have significance only for samples of porous beds containing a relatively large number of pores.

(a) Porosity (ϕ)

The porosity or void fraction of a material is the fraction of the bulk volume of the total material occupied by voids. Thus

$$\phi = \frac{\text{Volume of pores or void volume}}{\text{Total or bulk volume}} = \frac{V_p}{V_T} \qquad \text{(A1)}$$

The void fraction for randomly packed beds of uniformly sized spheres in containers

of diameters about 50 times the particle diameter is in the range of 0.36-0.43 [21].

(b) Equivalent diameter (d_v)

Porous unconsolidated material such as gravel beds are made up of pebbles with varying sizes and of irregular shape. The equivalent diameter is defined in terms of a mean spherical particle having the same volume. Thus

$$d_v = \left(\frac{6 \cdot V_s}{n\pi}\right)^{1/3} \tag{A2a}$$

where V_s is the volume of n particles selected randomly.

Alternatively, since V_s is not an easily measurable quantity, we can use the following expression to estimate d_v:

$$d_v = \left(\frac{6}{n\pi} \cdot (1-\phi) \cdot V_T\right)^{1/3} \tag{A2b}$$

Note that d_v is the mean diameter. For a more accurate treatment, the distribution of the particle diameters have to be determined experimentally for which purpose sieving is done using different sizes of screens.

(c) Particle shape factor (s)

The shape factor is important as it affects the surface area per unit volume and is usually defined in terms of a spherical particle which has the minimum surface area per unit volume. Thus

$$s = \frac{\text{surface area of a sphere per unit volume}}{\text{surface area of the particle}} \tag{A3}$$

(d) Effective diameter (d_s)

For purposes of friction drop or heat transfer calculations, it is the surface area (A_s) of the particles per unit volume of material which is the influencing parameter. Thus

$$A_S = \frac{n\pi d_v^2}{V_T} = \frac{\pi d_v^3 n}{6} \cdot \frac{6}{V_T . d_S} = (1-\phi) \cdot \frac{6}{d_S} \qquad (A4)$$

Following the hydraulic radii theory, the effective diameter can be computed as:

$$d_S = \frac{4 \text{ (void volume)}}{\text{wetted area}} = \frac{2}{3} \cdot \frac{\phi}{(1-\phi)} \cdot d_v \qquad (A5)$$

A2. Reynolds number

The Reynolds number, which is the ratio of inertia force to viscous force, gives an indication of the type of flow: whether laminar or turbulent. This is of crucial importance since pressure drop as well as heat transfer characteristics of the porous bed are greatly influenced by the regime under which flow occurs.

The Reynolds number is defined as

$$Re = \frac{q\rho}{A\mu} \cdot l = \frac{V.l}{\nu} \qquad (A6)$$

where V is the apparent or surface velocity, q the volumetric flow rate, ρ the fluid density, μ the dynamic viscosity, ν the kinematic viscosity, A the cross-sectional area of the porous bed and l a characteristic length dimension.

Note that V is not the actual velocity in the pores but is a velocity obtained by measuring the discharge q through an area A in the absence of the porous bed. It is often

referred to as the superficial velocity.

The question that arises is what to choose as the length dimension of the bed which should determine the nature of the flow. Different researchers seem to have chosen this dimension differently leading to a certain inconsistency in the corresponding Reynolds numbers thereby computed [16-18]. The most common definitions of the characteristic length for porous beds are:

(i) $l = d_s$

(ii) $l = d_v$

(iii) $l = (d_v/\phi)$

It must be pointed out that usually in flow through pipes, a dimension of the flow channel is chosen for l. However for porous beds it is difficult to measure pore or void diameter and consequently the particle or pebble diameter is preferred. However, this by itself does not explain all the characteristics of an actual porous bed with heterogeneous and irregular particles. Consequently in the present study we have opted to follow definition (iii). By including the porosity as well, the definition of the Reynolds number will actually correspond to the fluid velocity in the pores since this is given by (V/ϕ).

For the purposes of this study, we shall assume the following safe limits for the flow: laminar for $Re < 1$ and turbulent for $Re > 10$. Since the particles are irregular and of different sizes, the transition from laminar to turbulent flow is not abrupt at a single critical Reynolds number as is the flow through pipes. Instead the transition is rather gradual and therefore there exist studies which report laminar flows at Re values close to 5 and above, while others report the onset of turbulence at Re numbers close to 5. Thus the critical values stated above should be viewed as indicators for establishing the regime in an approximate manner rather than strict numerical cut-off values.

A3. Flow dynamics

The flow of fluids through porous media is complicated by the fact that the flow is highly irregular and tortuous. Despite this, the analogy to flow through pipes is used to study both laminar and turbulent regimes by starting explicitly with a correlation between Reynolds number and the friction factor. Consequently for porous media, the friction factor f can be defined as [17]:

$$f = d_v \cdot g \cdot \left(\frac{\phi A}{q}\right)^2 \cdot \frac{dp}{dx} \qquad \text{(A7)}$$

where dp is the pressure drop differential (Pa in SI units) across a porous bed length differential dx.

During the laminar regime, i.e. Re <1, the product (Re * f) is assumed to be essentially equal to a constant c. Thus, from eq.(A7) and the definition of Re, we have

$$\frac{q}{A} = g \cdot \frac{\phi . d_v^2}{c.\nu} \cdot \frac{dp}{dx} \qquad \text{(A8)}$$

where ν is the kinematic viscosity of the fluid flowing through the porous bed.

This equation is referred to as Darcy's law following the experimental scientist who originally proposed it. We can recast eq.(A8) as

$$\frac{q}{A} = K \cdot \frac{dp}{dx} \qquad \text{(A9)}$$

$$\text{where } K = g \cdot (\phi . d_v^2) / (c.\nu) \qquad \text{(A10)}$$

and is a coefficient representative of the conductivity of the porous bed to the particular fluid.

The parameter K depends on characteristic parameters of the porous bed as also (provided of course that the flow remains laminar) on those of the fluid (because of the inclusion of ν). In order to separate these, we define the permeability (sometimes also referred to as the 'intrinsic permeability') of the porous bed as

$$k = \frac{\phi \cdot d_v^2}{c} \tag{A11}$$

The conductivity K and the permeability are correlated as follows:

$$k = \frac{K \cdot c}{g} \tag{A12}$$

Thus the permeability can be defined as the volume of a fluid per unit viscosity passing through a unit cross section of the medium in unit time under the action of a unit pressure gradient [16]. It has units of area and is determined only by the structure of the porous bed and is entirely independent of the nature of the fluid. It is thus a constant for a bed made up of a specific porous material.

Finally, the following aspects need to be spelled out explicitly:

(i) The above derivation is intended more as a heuristic guide to understanding flow behavior rather than a formal proof of Darcy's law which most text books derive from the classical hydrodynamical equations of Navier-Stokes [20].

(ii) Equation (A11) is actually an operational definition of k. This is because the heterogeneity and irregularities of commonly encountered porous beds do not permit k to be accurately computed from basic properties of the bed which have to be

deduced experimentally. Thus the form of the equation suggests that a statistical averaging as against strict accounting for variation in flow in the individual pores has been adopted. Consequently, only on a macroscopic sense is the velocity of a fluid flowing through a porous medium directly proportional to the pressure gradiant acting on the fluid.

Darcy's law is no longer valid when the flow becomes partially or completely turbulent. Under such conditions, the literature contains several empirical models proposed by different researchers to treat flow in porous media. These are addressed briefly below.

(a) Linear dependence of (Re · f) on Re [16]:

This approach starts with the assumption that

$$Re \cdot f = c_1 + c_2 \cdot Re \tag{A13}$$

where c_1 and c_2 are dimensionless constants which depend on the properties of both fluid and porous media.

From the above, we obtain the relation

$$\frac{dp}{dx} = c_1' \frac{q}{A} + c_2' \left(\frac{q}{A}\right)^2 \tag{A14}$$

where c'_1 and c_2' are given by

$$c_1' = \frac{c_1.\nu}{g.d_v^2.\phi} \quad \text{and} \quad c_2' = \frac{c_2}{g.d_v.\phi^2} \tag{A15}$$

Such a treatment originally proposed by Forchheimer, has a certain amount of appeal

since it can simultaneously account for different types of flow while yielding the relative contributions of each on the total pressure drop. With $c'_2=0$, we get back Darcy's law while with $c'_1=0$, we obtain the quadratic exponent found for turbulent flow in pipes according to Fanning's equation. Thus we can view this approach as treating actual pressure drop as consisting of a pressure drop resulting from laminar flow added to a pressure drop occurring from turbulent flow.

(b) White and later Missbach [18] have suggested the following model:

$$Re \cdot f^n = c \tag{A16}$$

which is analogous to the following

$$\frac{dp}{dx} = a \cdot \left(\frac{q}{A}\right)^b \tag{A17}$$

where

$$a = \frac{1}{g} \cdot \left(\frac{c.\nu}{d_v^{n+1}.\phi^{2n-1}}\right)^{1/n} \quad \text{and} \quad b = \frac{2n-1}{n} \tag{A18}$$

It is clearly seen that for laminar flow b would be equal to 1 while for turbulent flow it would be close to 2. For mixed flow, the exponent would be between 1 and 2, the exact value being dependent on the circumstances specific to the particular case. Unlike the Darcy equation (eq.(A9)) where the interpretation of the constant k is unambiguous, it is difficult to assign a rigorous interpretation to the coefficients of eqs.(A13 & A16). However loosely speaking the coefficient a of eq.(A17) can be considered to represent the resistivity to flow offered by the porous media to the particular fluid.

Several other studies have proposed either variants of the above two approaches or

more complex empirical correlations, either between the Reynolds number and the friction factor, or directly for the pressure drop in the porous bed against parameters describing both material and flow conditions. We shall not discuss these here given the more advanced nature of these models and the inappropriateness of resorting to such models in the framework of the type of practical application we have in mind.

Appendix B: Experiments to Determine Porosity and Equivalent Diameters of Gravel

The porosity of a gravel bed (ϕ) and the equivalent diameter (d_v) of porous materials have been defined in Appendix A. Though these parameters do not explicitly figure in the pressure drop versus flow models outlined in the main portion of this report as also in Appendix A, they do implicitly influence such models through the permeability term of the porous bed. Thus a knowledge of these parameters would indeed be useful. Consequently we have undertaken an experimental determination of u and d_v, the results of which are presented and discussed below.

B1. Determination of bed porosity (ϕ)

Experimental techniques to determine porosity of porous beds are well known (see for example, Refs. [16,17]. Perhaps the simplest technique is to choose a certain volume of the bed material and then measure the volume of the voids by measuring the volume of a liquid (for example, water) needed to completely saturate the porous bed. Either the volume of liquid poured in or drained out (or both) could then be used to directly estimate the porosity.

Tables B1 and B2 present the experimental observations relating to the volume of water both poured in and then drained out from a total volume of the porous material of 1 liter. Note that the observations of the first run have to be discarded due to errors arising as a result of initial wetting of the gravel. Repetitions both in number of samples and runs for each sample assure the determination of a sounder and more representative value of ϕ.

We note that within-sample variance is smaller than that across samples for larger

Table B1. Experimental observations in order to determine porosity of the river-run gravel of 3/4" (0.019 m) nominal diameter. Numbers indicate volume of water in cubic centimeters poured in (1) and drained out (2) from a total volume of 1 liter.

Run	Sample A		Sample B		Sample C		Sample D		
	1	2	1	2	1	2	1	2	
1*	439	414	440	420	454	435	462	440	
2	424	425	415	415	447	447	427	426	
3	417	420	410	413	437	440	420	425	
4	412	415	414	416	434	439	422	425	
5	409	410	416	418	438	436	422	424	
Mean	416.5		414.6		439.7		423.9		423.7
SEM	2.16		0.84		1.71		0.83		5.72

(*) The values of this run are discarded due to initial wetting of the gravel

Table B2. Experimental observations in order to determine porosity of the river-run gravel of 1/2" (0.012 m) nominal diameter. Numbers indicate volume of water in cubic centimeters poured in (1) and drained out (2) from a total volume of 1 liter.

Run	Sample A		Sample B		Sample C		Sample D		Sample E		
	1	2	1	2	1	2	1	2	1	2	
1*	442	465	433	376	435	389	418	365	419	365	
2	378	384	376	381	394	392	375	374	374	375	
3	370	374	374	376	385	385	370	373	362	363	
4	368	370	372	375	376	377	371	374	366	368	
5	370	366	374	375	380	380	365	373	365	368	
Mean	372.5		375.4		383.6		371.9		367.6		374.2
SEM	2.10		0.92		2.35		1.14		1.14		2.66

(*) The values of this run are discarded due to initial wetting of the gravel.

gravel which suggests that the errors of our experimental procedure are lower than the variations associated with taking different samples. Though this is not so for the smaller gravel, the magnitude of these values are small and can be confidently overlooked for our purpose.

We summarize the values of the porosity estimated for river run gravel:

0.012 m (1/2 in.) nominal diameter: = 0.374

0.019 m (3/4 in.) nominal diameter: = 0.424.

B2. Determination of equivalent diameter (d_v)

The most convenient way of deducing d_v is from eq.(A2b). Since we already have an estimate of the porosity, all that remains is to determine the number of gravel stones in a given volume.

Again we chose a total volume of 1 liter and counted the number of stones, the results of which are shown in Table B3. It would have been better to get an estimate of the particle size distribution as well, but this could not be done due to lack of appropriate screening sieves. Thus only an estimate of the mean diameter has been obtained in this study.

The mean number of pebbles in both sizes of gravel are given in Table B3 along with the SEM values. We note that for large gravel the SEM is almost 5% while for smaller gravel it is less: something which is to be expected given that experimental errors are larger for larger gravel.

The mean values of d_v computed from the experimental readings of Table B3 are:

Table B3. Results of the experiment to determine the mean equivalent particle diameter of the river-run gravel. Total volume of the sample was 1 liter.

Sample No.	Large pebbles Nominal diameter = 3/4" (0.019 m) No. of pebbles	Small pebbles Nominal diameter =1/2" (0.012m) No. of pebbles
1	209	1458
2	179	1688
3	174	1529
4	181	-
Mean	185.75	1558.3
SEM	7.89	68.0

River-run gravel	Nominal diameter	Estimated equivalent diameter
Large	0.019 m (3/4 in.)	0.018 m (0.71 in.)
Small	0.012 m (1/2 in.)	0.009 m (0.36 in.)

We note that deviation between nominal and equivalent diameters is small for the large river-run gravel. As for the smaller sized gravel, the important difference is likely to be as a result of the fact that this gravel type contained a relatively large number of very small pebbles thereby decreasing the estimated effective mean value. Thus we attribute this departure from the nominal diameter to have arisen as a result of improper or non-rigorous sieving separation process adopted by the supplier rather than as a result of the pebbles being systematically smaller. A fact to be retained is that in practical situations, the large variation in the distribution of particle diameters even when a specific nominal diameter is specified would lead to a loss of scientific predictability or reproducibility in the pressure drop versus flow relationships when these are estimated from actual experimental measurements.

Appendix C: Quality Assurance and Quality Control (QA/QC) Statement

Data, in general, have been collected in accordance with the data quality goals set forth in the QAPP section of Ref. 22. We shall, however, address in this appendix the measurements specifically relevant in the framework of this particular study.

Two types of experiments were performed: one in the laboratory setting (described in Section 5) and another in an actual research house (described in Section 7). Both these types of experiments essentially involved the use of the same types of instruments and of data gathering techniques. Consequently, the discussion that follows applies to both these experimental settings.

Equipment used are described below:

(i) an industrial vacuum cleaner capable of sucking 45×10^{-3} m^3/s (95 cfm) of air through a 0.05 m (2 in.) diameter orifice under 1.9 m (75 in.) of water static vacuum pressure;

(ii) a speed control and an air by-pass adapter (which is simply a perforated length of plastic pipe). Both these are needed in order to vary the air flow rate through the porous bed;

(iii) a 3 mm stainless steel pitot-tube (Dwyer No. 166-6) to measure velocities from 0.05 to 15 m/s (10 to 3000 ft/min). Tables for different pipe diameters (as described in Ref. [4]) enabled the corresponding volume flow rate to be deduced;

(iv) an electric digital micromanometer (EDM) (Neotronics Model EDM-1) which can measure pressures with a resolution of 0.025×10^{-3}m (10^{-3} in.) of water or 0.25 Pa, and having a maximum range of up to 0.5 m (20 in.) of water. This is also described in Ref. [4].

(v) two mounting devices: (a) a 0.038 m (1.5 in.) outer diameter brass pipe to connect the

suction hole to the vacuum hose with arrangements to attach the pitot tube [called the Flow Pressure Tube (FPT)], and also the EDM, and (b) a 0.019 m (0.75 in.) stainless steel pipe to mount the EDM in order to measure the pressure at each of the nine different taps. These devices have already been described in detail in a previous report [4].

Details of the accuracy, precision and completeness as well as the calibration details are given in Table C1. The data gathered was discrete in nature (as against data electronically measured and stored continuously in a data logger). For the laboratory experiments, three sets of experiments were conducted (see Table 1). In all, 9 discrete runs of data gathering were involved, with each run entailing one air flow rate measurement and 9 pressure difference measurements. During field experiments in the research house, only 3 discrete runs were performed, each run requiring the measurement of one air flow rate and 19 pressure difference measurements. Care was taken in both experimental settings that all data gathered were in accordance with the particular QAPP and met those requirements. How the data collected was analyzed is described in Sections 5 and 7 of the main portion of this study.

Table C1. Monitoring Instruments

Instrument	Range	Accuracy	Precision	Completeness	Calibration Standard	Frequency of Calibration	
						Zero	Span
1. Pitot-tube Dwyer No. 166-6	0.05-15 m/s	5%	5%	95%	Factory	Before each measurement	1/6 months
2. Electric Digital Micromanometer, Neotronics Model EDM-1	0-5000 Pa	0.25 Pa	0.25 Pa	95%	Factory	Before each measurement	1/6 months